Lysine deacetylation inhibition reverses TDP-43 mislocalization and in combination with arimoclomol ameliorates neuromuscular pathology

Serena Scozzari[1#], Stefano Fabrizio Columbro[1#], Monica Favagrossa[1], Massimo Tortarolo[1], Alfredo Cagnotto[2], Mario Salmona[2], Giovanni De Marco[3], Caterina Bendotti[1], Andrea Calvo[3], Laura Pasetto[1*], and Valentina Bonetto[1*]

[1]Research Center for ALS, Istituto di Ricerche Farmacologiche Mario Negri IRCCS, Milano, Italy

[2]Department of Biochemistry and Molecular Pharmacology, Istituto di Ricerche Farmacologiche Mario Negri IRCCS, Milano, Italy

[3]"Rita Levi Montalcini" Department of Neuroscience, Università degli Studi di Torino, Torino, Italy

[#]These are co-first authors

*These are co-corresponding authors

Abstract

Background: Cytoplasmic inclusions containing TAR DNA-binding protein 43 kDa (TDP-43) are recognized as a major pathological feature of amyotrophic lateral sclerosis (ALS) and frontotemporal dementia, but more recently have been associated with several neurodegenerative conditions. Cyclophilin A (PPIA), a foldase and molecular chaperone, interacts with TDP-43 and influences its aggregation and function. The interaction between PPIA and TDP-43 is facilitated by PPIA Lys-acetylation, which is reduced in peripheral blood mononuclear cells (PBMCs) of ALS patients showing signs of TDP-43 proteinopathy. In this study, we investigated the effect of lysine deacetylation inhibition to uncover the underlying mechanisms of TDP-43 proteinopathy in relation to PPIA acetylation, and to identify new therapeutic avenues.

Methods: Through a screening of histone deacetylase (HDAC) inhibitors in a cellular model of TDP-43 proteinopathy, we identified vorinostat/SAHA, capable of increasing PPIA acetylation, as the most effective in reversing TDP-43 mislocalization. We confirmed its effect in PBMCs from ALS patients. Next, we explored its impact on proteinopathy and PPIA acetylation in a severe and fast-progressing TDP-43-overexpressing mouse model (Thy1-hTDP-43), using several molecular biomarkers as outcome measures, including neurofilament light chain (NfL) in plasma.

Results: Thy1-hTDP-43 mice treated with SAHA showed a delayed onset of TDP-43 pathology, associated with PPIA nucleus-cytoplasm redistribution, lower levels of neurodegeneration and neuroinflammation markers, and improved neuromuscular function markers. However, over time, the broad-spectrum inhibitor SAHA was unable to counteract the two-fold overexpression of TDP-43 and led to the accumulation of side effects. When combined with the heat shock protein (HSP) co-inducer arimoclomol, a mitigation of the neurodegeneration was sustained. Moreover, a synergistic effect was observed in periphery, greatly enhancing tubulin acetylation and reducing pTDP-43 accumulation in the sciatic nerve. This resulted in a more pronounced reduction of NfL in plasma and acetylcholine receptor (AChR) γ-subunit expression in gastrocnemius muscle, indicating reduced axonal transport impairment and muscle denervation.

Conclusions: This study suggests that HDAC inhibition, by increasing acetylated PPIA, could be beneficial in restoring TDP-43 localization and function. The combination of lysine deacetylation inhibition and HSP induction shows a synergistic effect *in vivo* and has potential as a therapeutic approach for patients.

Keywords

TDP-43 proteinopathy; Lys-acetylation; HDAC inhibitors; HSP co-inducer; Peptidyl-prolyl cis/trans isomerase

Background

Cytoplasmic inclusions containing TAR DNA-binding protein 43 kDa (TDP-43) were originally discovered in affected central nervous system (CNS) regions of patients with amyotrophic lateral sclerosis (ALS) and frontotemporal lobar degeneration [1]. Since then several studies have contributed to establish TDP-43 inclusions as a major pathological component of ALS and frontotemporal dementia (FTD), and mutations in *TARDBP*, the gene encoding for TDP-43, have been found to cause familial ALS, ALS-FTD and FTD, although rarely. More recently, intraneuronal cytoplasmic inclusions of TDP-43 have also been seen in the brain of more than 50% of Alzheimer's (AD) disease patients [2], about 25% of elderly individuals, as limbic-predominant age-related TDP-43 encephalopathy neuropathological changes [3], and 40% of subjects with chronic traumatic encephalopathy linked to repetitive head injuries [4], Parkinson's [5] and Huntington's disease [6]. These later discoveries have broadened the range of TDP-43-related conditions [7] and underscored the importance of understanding the molecular mechanisms behind this pathology for developing effective treatments.

TDP-43 is an RNA-binding protein normally localized in the nucleus, also capable of shuttling to the cytoplasm, to govern various cellular functions such as transcriptional repression, pre-mRNA splicing, mRNA stability, microRNA biogenesis, RNA transport, and translational regulation [8]. While the precise pathological function of TDP-43 remains elusive, mounting evidence suggests that its depletion from the nucleus and its accumulation in the cytoplasm can result in both gain and loss of functions. Due to its aggregation propensity, cells tightly regulate TDP-43 levels by an auto-regulatory feedback loop involving its own mRNA transcript [9,10] and, upon stress conditions, activate protective mechanisms by which transiently store TDP-43 into liquid-liquid phase-separated droplets in the nucleus and the cytoplasm [11–13]. Under prolonged stress conditions, the coping response fails and TDP-43 accumulates as aggregates mainly in the cytoplasm likely causing nucleocytoplasmic transport impairment, clearance of nuclear TDP-43, impaired splicing function, deficient axonal transport and cell death [14–17].

Peptidyl-prolyl cis-trans isomerase A (PPIA), a foldase and molecular chaperone, interacts with TDP-43 and impacts on its aggregation [18,19]. Under stress conditions, PPIA has been found associated with membrane-less assemblies in the cytoplasm [12,20,21] and in the nucleus [11], and there is evidence that it regulates liquid-liquid phase separation of its substrates [22,23]. Moreover, it has been found sequestered in protein aggregates in ALS patients and mouse models [18,24]. PPIA knockout mice develop a neurodegenerative disease which resembles ALS-FTD with marked TDP-43 pathology [19]. PPIA depletion in $SOD1^{G93A}$ mice induces TDP-43 aggregation and accelerates disease progression [18]. The interaction between PPIA and TDP-43 occurs at the Gly-Pro dipeptide motif (residues 348-349) in the C-terminal Gly-rich domain of TDP-43 that has prion-like properties, and is favored by PPIA acetylation at K125 [18]. PPIA Lys-acetylation is low in cells under stress conditions and in peripheral blood mononuclear cells (PBMCs) of ALS patients [18], where signs of TDP-43 proteinopathy have been found [25,26]. Moreover, we identified a PPIA loss-of-function K76E mutation, at a Lys susceptible to acetylation [27], in a patient with sporadic ALS

[19]. However, it is not known if modulating PPIA acetylation has an effect on TDP-43 aggregation and function.

The level of Lys-acetylation decreases globally in neurons during neurodegeneration, reflecting an impairment in the acetylation homeostasis [28]. The removal of acetyl groups is mediated by histone deacetylases (HDACs), a superfamily of enzymes grouped in four classes, now also named lysine deacetylases in consideration of the numerous non-histone protein targets recently identified [29]. HDAC inhibitors (HDACis) have shown to have interesting neuroprotective effects for ALS and in general for neurodegenerative diseases [30,31]. Nevertheless, the pan HDACis tested in clinical studies for ALS, valproic acid and sodium phenylbutyrate, had no beneficial effects [32,33], probably because having a broad spectrum of action have also harmful effects [34,35]. Novel, more specific, molecules are now available. HDAC3 specific inhibitor RGFP966 regulated the expression of the amyloid precursor protein and promoted neuroprotective pathways in an AD mouse model [36]; tubastatin A and ACY-738, HDAC6 specific inhibitors, reversed axonal transport defects in FUS mice and in motor neurons derived from ALS patients, carrying FUS and TDP-43 mutations [15,37,38]; selisistat, a specific SIRT1 inhibitor, counteracted mutant SOD1 toxicity in neuronal cells [39]; the broad-spectrum inhibitor vorinostat, also known as suberoylanilide hydroxamic acid (SAHA), or the HDAC1/3 inhibitor RGFP109 induced heat shock protein (HSP) response in motor neurons expressing variants linked to familial ALS and potentiate efficacy of the HSP co-inducer arimoclomol [40,41].

In this study, we investigated the effect of lysine deacetylation inhibition in cellular and mouse models of TDP-43 proteinopathy and in PBMCs of ALS patients. The aim was to uncover the underlying mechanisms of TDP-43 proteinopathy in relation to PPIA acetylation and identify possibly new therapeutic avenues.

Methods

Drugs

Drugs for cells and mice treatments were purchased from MedChemExpress and were as follows: SAHA (HY-10221), RGFP109 (HY-16425), RGFP966 (HY-13909); ACY-738 (HY-19327); tubastatin A (HY-13271A), selisistat (HY-15452), arimoclomol maleate (HY-106443A).

Antibodies

Antibodies used for immunoblot (dot/WB) and capillary electrophoresis immunoassay (CEI) on Jess (Protein Simple, Biotechne) were as follows: rabbit polyclonal anti-C-terminal TDP-43 antibody (1:2500 for immunoblot, 1:20 for Jess; Proteintech; RRID: AB_2200505), rabbit polyclonal anti-acetyl-PPIA (Lys125) antibody (1:250 for immunoblot, 1:10 for Jess; developed in-house), rabbit polyclonal anti-PPIA antibody (1:2500 for immunoblot, 1:40 for Jess; Proteintech; RRID: AB_2237516), mouse monoclonal anti-acetyl alpha-tubulin (Lys40) antibody (1:1000 for immunoblot; Sigma-Aldrich; RRID: AB_609894); mouse monoclonal anti-alpha tubulin antibody (1:1000 for immunoblot; Santa Cruz Biotechnology; RRID: AB_628412); mouse monoclonal anti-phospho-Ser409/410 TDP-43 antibody (pTDP-43) (1:2000 for

immunoblot; Cosmo Bio Co., LTD; RRID: AB_1961900), rabbit polyclonal anti-HSP70 antibody (1:20000 for immunoblot; Proteintech; RRID: AB_2264230).

Dot blot and Western Blot (WB)

Protein levels were determined using the Pierce™ BCA Protein Assay Kit (Thermo Fisher Scientific). For WB, samples (15-20 µg) were separated in 12% SDS-polyacrylamide gels and transferred to polyvinylidene difluoride membranes (0.45 µm; Millipore), as described previously [24]. For dot blot, proteins (3 µg) were loaded directly onto nitrocellulose Trans-blot transfer membranes (0.45 µm; Bio-Rad), depositing each sample on the membrane by vacuum filtration, as described previously [26]. WB and dot blot membranes were blocked with 3% (w/v) BSA (Sigma-Aldrich) and 0.1% (v/v) Tween 20 in Tris-buffered saline, pH 7.5, and incubated with primary antibodies and then with peroxidase-conjugated secondary antibodies (GE Healthcare). Blots were developed with the Luminata Forte Western Chemiluminescent HRP Substrate (Millipore) on the ChemiDoc™ Imaging System (Bio-Rad). Densitometry was done with Image Lab 6.0 software (Bio- Rad). The immune reactivity of the different proteins was normalized to Ponceau Red staining (Fluka).

Capillary electrophoresis immunoassay (CEI)

CEI was performed on the Jess instrument (Protein Simple, Biotechne). Samples diluted in 0.1X Sample Buffer to 0.2-2 µg/µl concentrations, added to the Fluorescent Master Mix and incubated for 5 min at 95 °C. Samples, antibodies and reagents were loaded in the plate following the "Immunoassay + Total Protein" template and plate was centrifuged at 1000 x *g* for 5 min at RT, according to the manufacturer's instructions. 12–230 kDa separation module with 25-capillary cartridge was employed and chemiluminescent detection with RePlex and Total Protein assay was run. Target proteins are normally observed to be approximately 10 kDa higher than in standard WB, as described [42]. Data were analysed using Compass for Simple Western 6.3.0 software and immunoassay data were corrected for total protein signal.

***In vitro* model of TDP-43 pathology and treatments**

HEK293 cells were cultured in DMEM GlutaMAX (Dulbecco's Modified Eagle Medium with L-Glutamine) (Gibco) containing 10% fetal bovine serum (FBS) (Sigma-Aldrich), 1% non-essential amino acids (Gibco) and 1% penicillin/streptomycin (Gibco) and maintained at 37°C in a humidified atmosphere and 5% CO_2. To induce TDP-43 pathology, HEK293 cells were exposed to a chronic nutrient starvation protocol, essentially as previously described [43]. Briefly, cells were seeded in a complete medium for 24 hours, becoming 70% confluent; the following day, FBS deprived medium was replaced and nutrient starvation was carried out for 72 hours. The cellular model was used as a biological platform for the pharmacological screening. Cells were seeded in a complete medium and subjected to overnight pre-treatment with 0.6 µM or 1 µM HDACis: SAHA, RGFP109, RGFP966, ACY-738, tubastatin A or selisistat. The following day, cells were exposed to the chronic nutrient starvation protocol, collected after 72 hours, and stored as pellet at -70 °C until further analysis.

ALS patients

Informed written consent was obtained from all participants involved and the study was approved by the ethics committee of Azienda Ospedaliero-Universitaria Città della Salute e della Scienza, Turin, Italy. The diagnosis of ALS was based on a detailed medical history and physical examination, and confirmed by electrophysiological evaluation. The patients were screened for mutations in the SOD1, C9orf72, TARDBP, and FUS genes. Inclusion criteria for ALS patients were: (i) 18–85 years old; and (ii) had a diagnosis of definite, probable or laboratory-supported probable ALS, according to revised El Escorial criteria. Exclusion criteria were: (i) diabetes or severe inflammatory conditions; (ii) active malignancy; and (iii) pregnancy or breast-feeding. ALS patients underwent a battery of neuropsychological tests and were classified according to the consensus criteria for the diagnosis of frontotemporal cognitive and behavioral syndromes in ALS. We analyzed clinical samples from nine ALS patients and 54 healthy controls. The characteristics of the patients and controls are described in Table 1.

Human PBMC isolation and treatment

Blood was drawn by standard venipuncture at the clinical center, collected in 4-ml BD Vacutainer® CPT™ Mononuclear Cell Preparation Tubes - Sodium Citrate and PBMCs were isolated following the manufacturer's protocol. PBMCs were then subjected to three additionally washing steps in phosphate buffer saline and centrifugation at 300 x *g* for 15 min at RT. PBMCs were stored at -70°C until further analysis, as pellet for biomarkers analysis or in 90% FBS and 10% dimethyl sulfoxide for *in vitro* experiments. For PBMCs culture and treatment, cells were quickly thawed in a 37°C water bath, diluted 1:10 in warm RPMI medium 1640 (Gibco) and collected by centrifugation at 300 x *g* for 15 min at RT. Cells were cultured at a final concentration of 1100000 cells/ml in complete RPMI medium 1640 (Gibco), containing 10% FBS (Sigma-Aldrich), 1% L-glutamine (Carlo Erba Reagents) and 1% penicillin/streptomycin (Gibco). PBMCs isolated from each patient were split in two cultures, one subjected to overnight treatment with 1 µM SAHA, the other group maintained as untreated control; cells were incubated overnight at 37°C in a humidified atmosphere and 5% CO_2.

Subcellular fractionation in HEK293 cells, human PBMCs and mouse spinal cord.

HEK293 cells were lysed in ice-cold RIPA buffer (0.3% Triton X-100, 50 mM Tris-HCl pH 7.4, 1 mM EDTA) and cOmplete™ Protease Inhibitor Cocktail Tablets (Roche, 1 tablet/10 ml buffer), with rotation at 4°C for 30 min, as previously described [18]. Cell extracts were centrifuged to pellet nuclei at 12000 x *g* for 10 min at 4°C and the supernatant was collected in a new tube as cytoplasmic fraction. Nuclear pellet was washed by gently resuspension in ice-cold RIPA buffer and centrifuge at 10000 x *g* for 5 min at 4°C. PBMCs were lysed essentially as described by Miskolci *et al*. [44]. Pellets were suspended in ice-cold buffer containing 10 mM Hepes pH 7.5, 10 mM KCl, 3 mM NaCl, 3 mM $MgCl_2$, 1 mM EDTA pH 8.8, 1 mM EGTA and cOmplete™ Protease Inhibitor Cocktail Tablets (Roche, 1 tablet/10 ml buffer) and kept on ice for 15 min. Samples were treated by adding NP-40 at a final concentration of 0.5 %, vortexed and kept on ice for 8 sec, then centrifuged to pellet nuclei at 850 x *g* for 5 min at 4°C, while the supernatant was collected in a new tube as cytoplasmic

fraction. Nuclear pellet was resuspended in ice-cold RIPA buffer and centrifuge at 2400 x *g* for 5 min at 4°C. Nuclear and cytoplasmic fractions were isolated from mouse spinal cord as described [19]. Briefly, tissues were homogenized in six volumes (w/v) of buffer A (10 mM Tris-HCl pH 7.4, 5 mM $MgCl_2$, 25 mM KCl, 0.25 M sucrose, 0.5 mM DTT) with cOmplete™ Protease Inhibitor Cocktail Tablets (Roche, 1 tablet/10 ml buffer), and centrifuged at 800 x *g* for 10 min at 4°C. The supernatant (cytoplasmic fraction) was centrifuged at 800 x *g* for 10 min at 4°C to remove fraction contamination. The pellet was resuspended in buffer A, centrifuged at 800 x *g* for 10 min at 4°C, subsequently resuspended in one volume of buffer A and one volume of buffer B (10 mM Tris-HCl pH 7.4, 5 mM $MgCl_2$, 25 mM KCl, 2 M sucrose, cOmplete™ Protease Inhibitor Cocktail Tablets (Roche, 1 tablet/10 ml buffer) and loaded on a layer of one volume of buffer B. Samples were ultracentrifuged at 100000 x *g* for 45 min at 4°C and the pellet (nuclear fraction) was resuspended in 100 µL of buffer A, centrifuged at 800 x *g* for 10 min at 4°C and resuspended in 40 µL buffer A. For both HEK293 cells, human PBMCs and mouse spinal cord cytoplasmic and nuclear fractions were lysed by adding pre-warmed at 95°C SDS at a final concentration of 1% and shaken at 800 rpm for 5 min at 95°C. Nuclei were then sonicated for 30 sec at RT.

Total protein extraction in HEK293 cells, human PBMCs, mouse spinal cord and sciatic nerve.

HEK293 cells, human PBMCs or lumbar spinal cord were lysed in pre-warmed at 95 °C buffer containing 1% SDS, cOmplete™ Protease Inhibitor Cocktail Tablets (Roche), shaken at 800 rpm for 5 min at 95°C in the Thermomixer and DNA complexes were disrupted using a 25-gauge needle of a 1 ml syringe. Samples were centrifuged at 9000 x *g* for 15 min at RT and supernatant was collected in a new tube as total protein extract. The extraction of total protein from sciatic nerves was carried out as reported [45]. Briefly, sciatic nerve was homogenized in ice-cold lysis buffer (50 mM Tris-HCl pH 8, 150 mM NaCl, 5 mM EGTA, 2 mM $MgCl_2$, 1% of Triton X-100, 10% anhydrous glycerol, protease and phosphatase inhibitors), sonicated, centrifuged at 18000 x *g* for 15 min at 4°C and supernatant was collected as total protein extract.

HDAC mRNA silencing

For RNA interference experiments in HEK293 cells, a reverse transfection protocol was applied. Complexes were prepared in 24-wells plate by diluting 6 pmol of siRNA for *HDAC1* (5'-UGG CCA UCC UGG AAC UGC UAA AGU A-3'; ID: HSS104726; Invitrogen) or siRNA for *HDAC3* (5'-CAA GGA AAG CGA UGU GGA GAU UUA A-3'; ID: HSS189614; Invitrogen) or scrambled siRNA (Stealth™ RNAi Negative Control Duplex #12935-113; Invitrogen) in Opti-MEM™ I Reduced Serum Medium (Gibco) with Lipofectamine™ RNAiMAX Transfection Reagent (Invitrogen). After a 15 min incubation at RT, cells were diluted in complete growth medium without antibiotics, added to each well and incubated for 24 hours at 37°C in a humidified atmosphere and 5% CO_2, according to the manufacturer's protocol. Gene silencing was confirmed by immunoblot analysis.

Generation and purification of an anti-K125 acetylated PPIA (PPIAK125ac) polyclonal antibody

For the preparation of polyclonal antibodies, the peptide WLDGKHVVFG acetylated at the K residue was synthesized by solid-phase peptide synthesis on an automated Alstra synthesizer (Biotage, Uppsala, Sweden) at 0.1 mM scale on tetravalent multiple antigenic peptide resin (MAP) resins using Fmoc-protected L-amino acids (Sigma Aldrich, Laufelfingen, CH) [46]. Amino acids were activated by a reaction with O-(Benzotriazole-1-yl)-N, N, N', N'-tetramethyluronium tetrafluoroborate, and N, N-diisopropylethylamine. A capping step with acetic anhydride was included after the last coupling cycle of each amino acid. The peptide was cleaved from the resin with trifluoroacetic acid/thioanisole/water/ phenol/ethanedithiol (82.5:5:5:5:2.5 vol/vol), precipitated, and washed with diethyl ether. The peptide was purified by reverse-phase high-performance liquid chromatography on a semi-preparative C18 column (Waters Corporation, Milford, MA), and its identity was confirmed with a MALDI-TOF spectrometer (Applied Biosystems, Concord, Ontario, Canada). The peptide purity was higher than 95%. The samples were then freeze-dried and stored at −20 °C until use. The polyclonal antibodies production was carried out by the Company Biogem, Ariano Irpino, Avellino (Italy). Immunization was performed by subcutaneous injection of the MAP peptide in White New Zealand rabbits, and the titer was measured by ELISA on serum samples. A highly specific antibody for the acetylated form of PPIA was obtained through a two-step affinity purification process using the Pierce™ NHS-Activated Agarose kit (Catalog #26198). Initially, the serum was deprived of antibodies that recognize the peptide corresponding to the amino acids of PPIA from position 121 to 130, but whose K125 was not acetylated. The resulting serum was then further affinity-purified, performing positive selection by resin functionalization with the same peptide used for rabbit immunization, acetylated at K125.

Thy1-hTDP-43 mouse model

Procedures involving animals and their care were conducted in conformity with the following laws, regulations, and policies governing the care and use of laboratory animals: Italian Governing Law (D.lgs 26/2014; Authorization 19/2008-A issued 6 March, 2008 by Ministry of Health); Mario Negri Institutional Regulations and Policies providing internal authorization for persons conducting animal experiments (Quality Management System Certificate, UNI EN ISO 9001:2015 - Reg. N° 6121); the National Institutes of Health's Guide for the Care and Use of Laboratory Animals (2011 edition), and European Union directives and guidelines (EEC Council Directive, 2010/63/UE). The Mario Negri Institutional Animal Care and Use Committee and the Italian Ministry of Health (Direzione Generale della Sanita` Animale e dei Farmaci Veterinari, Ufficio 6) prospectively reviewed and approved the animal research protocols of this study (protocol N° 9F5F5.139) and ensured compliance with international and local animal welfare standards. The Thy1-hTDP-43 mouse line on a homogeneous C57BL/6J background derives from the B6;SJL-Tg(Thy1-TARDBP)4Singh/J line originally obtained from The Jackson Laboratory (Stock N° 012836; Bar Harbor, ME, USA), which expresses 2 copies of human *TARDBP*. Transgenic Thy1-hTDP-43 mice were generated by breeding male and female hemizygous TDP-43 mice. Mice homozygous for TDP-43 in the C57BL/6J background exhibited overexpression of TDP-43 in neurons beginning at seven days of age (pre-symptomatic stage), at 14 days of age (disease onset) show abnormal hindlimb clasping reflex, with severe motor

impairment at 17 days of age (symptomatic stage) [47]. Genotyping for *TARDBP* was done by standard PCR on DNA phalanx biopsies, using primer sets designed by The Jackson Laboratory. Animals were bred and maintained at the Istituto di Ricerche Farmacologiche Mario Negri IRCCS, Milan, Italy, under standard conditions: temperature 21 ± 1°C, relative humidity 55 ± 10%, 12h light schedule, and food and water *ad libitum*. For tissue and plasma collection, animals were deeply anesthetized with ketamine hydrochloride (IMALGENE, 100 mg/kg; Alcyon Italia) and medetomidine hydrochloride (DOMITOR, 1 mg/kg; Alcyon Italia) by intraperitoneal injection and killed by decapitation. The number of animals was calculated on the basis of experiments designed to reach a power of 0.8, with a minimum difference of 20% ($\alpha = 0.05$).

Extraction of detergent-insoluble proteins

For detergent-insoluble protein extraction, spinal cord was homogenized in 10 volumes (w/v) of buffer (15 mM Tris–HCl pH 7.6, 1 mM dithiothreitol, 0.25 M sucrose, 1 mM $MgCl_2$, 2.5 mM EDTA, 1 mM EGTA, 0.25 M Na_3VO_4, 2 mM $Na_4P_2O_7$, 25 mM NaF, 5 µM MG132, cOmplete™ Protease Inhibitor Cocktail Tablets (Roche, 1 tablet/10 ml buffer) as described [19]. Briefly, the samples were centrifuged at 10000 x *g*, and the pellet was suspended in an ice-cold homogenization buffer containing 2% Triton X-100 and 150 mM KCl. The samples were then centrifuged at 10000 x *g* to obtain the Triton-insoluble (insoluble) fraction.

Plasma neurofilament light chain and matrix metalloproteinase-9 (MMP-9) quantification

Mouse plasma samples were collected in K2-EDTA BD Microtainer blood collection tubes and centrifuged at 5000 x *g* for 5 min to obtain the plasma. The plasma neurofilament light chain (NfL) was quantified using a Simoa NfLight Advantage (SR-X) Kit (#103400) on a Quanterix SR-X platform (Quanterix, Boston, MA, USA). The level of MMP-9 in plasma was measured with an AlphaLISA kit for the murine protein (#AL519, PerkinElmer). AlphaLISA signals were measured using an Ensight Multimode Plate Reader (PerkinElmer). All reagents used for NfL and MMP-9 analysis were from a single lot, and measurements were performed according to the manufacturer's protocol.

Quantitative real-time polymerase chain reaction

Total RNA from gastrocnemius muscle and spinal cord was extracted using Trizol (Invitrogen, Waltham, MA, USA) and purified with PureLink RNA columns (Life Technologies, Carlsbad, CA, USA). RNA samples were treated with DNase I and reverse transcribed with the High-Capacity cDNA Reverse Transcription Kit (Life Technologies, Carlsbad, CA, USA). For quantitative real-time polymerase chain reactions (RT-PCR), we used the Taq Man Gene expression assay (Applied Biosystems, Waltham, MA. USA), on cDNA specimens in triplicate, using 1X Universal PCR master mix (Life Technologies, Carlsbad, CA, USA) and 1X mix containing specific receptor probes for mouse acetylcholine receptor (*AChR*) *γ*-subunit in muscle (Mm00437419_m1; Life Technologies, Carlsbad, CA, USA), microtubule associated protein 2 (*Map-2*) (Mm00485231_m1; Life Technologies, Carlsbad, CA, USA) and *Hdac1* (*Mm02745760*_g1; Life Technologies, Carlsbad, CA, USA), *Hdac2* (Mm00515108_m1; Life Technologies, Carlsbad, CA, USA),

Hdac3 (Mm00515916_m1; Life Technologies, Carlsbad, CA, USA), *Hdac4* (Mm01299557_m1; Life Technologies, Carlsbad, CA, USA) and *Hdac6* (Mm00515945_m1; Life Technologies, Carlsbad, CA, USA) in spinal cord. Relative quantification was calculated from the ratio of the cycle number (Ct) at which the signal crossed a threshold set within the logarithmic phase of the given gene to that of the reference mouse *β-actin* gene (Mm02619580_g1; Life Technologies, Carlsbad, CA, USA). The means of the triplicate results for each sample were used as individual data for $2^{-\Delta\Delta Ct}$ statistical analysis.

Skiptic and cryptic exon analysis

Total RNA from spinal cord was extracted using Trizol (Invitrogen, Waltham, MA, USA) and purified with PureLink RNA columns (Life Technologies, Carlsbad, CA, USA). RNA samples were treated with DNase I and reverse transcribed with the High-Capacity cDNA Reverse Transcription Kit (Life Technologies, Carlsbad, CA, USA). For the evaluation of skiptic exon Ankrd42, Ube3C, Slc6a6, Plod1, Pex16, Pacrgl, Herc2 and of cryptic exon 2610507B11Rik, Adipor2, A230046K03Rik, Adnp2, Celf5 in spinal cord semi-quantitative PCR was performed on cDNA with specific primers spanning the differentially expressed exon. Products were electrophoresed on 8% polyacrylamide gel and using GelRed (Merck Millipore) staining results were visualized on a ChemiDoc Imaging System (Bio-Rad, Hercules, CA, USA). Results were analysed using the percentage of exon exclusion (PEE) measure, calculated dividing the intensity of the exon exclusion band by the sum of both exon inclusion and exon exclusion bands. Primer sequences are reported in Supplementary Table 1.

Immunohistochemistry

Mice were anesthetized and perfused transcardially with 50 mL of phosphate-buffered saline (PBS) followed by 100 mL of 4% paraformaldehyde (Sigma-Aldrich) in PBS. Spinal cord was rapidly removed, postfixed for 3h, transferred to 20% sucrose in PBS overnight and then to 30% sucrose solution until they sank, frozen in N-pentane at 45°C and stored at -80°C. Before freezing, spinal cord was divided into cervical, thoracic, and lumbar segments and included in Tissue-tec OCT compound (Sakura). Coronal sections (30 µm; four slices per mouse) of lumbar spinal cord were then sliced and immunohistochemistry was done. Rat monoclonal anti-CD11b antibody (1:800, Bio-Rad; RRID: AB_ 321292) was used for immunohistochemistry analysis. Briefly, slices were incubated for 1h at RT with blocking solutions (0.3% Triton X100 plus 10% NGS), then overnight at 4°C with the primary antibodies. After incubation with biotinylated secondary antibody (1:200; 1h at RT; Vector Laboratories) immunostaining was developed using the avidin–biotin kit (Vector Laboratories) and diaminobenzidine (Sigma). Coronal lumbar spinal cord (30 µm; twelve slices per mouse) were stained with 0.5% cresyl violet to detect the Nissl substance of neuronal cells. Stained sections were collected at 20 X and 40 X with an Olympus BX-61 Virtual Stage microscope so as to have complete stitching of the whole section, with a pixel size of 0.346 µm. Acquisition was done over 6-µm-thick stacks with a step size of 2 µm. The different focal planes were merged into a single stack by mean intensity projection to ensure consistent focus throughout the sample. Finally, signals were analysed for each slice with ImageJ and OlyVIA software.

Preclinical studies in the Thy1-hTDP-43 mouse model

Thy1-hTDP-43 mice received 50 mg/kg dose of SAHA, 10 mg/kg dose of arimoclomol (Arim.), 50 mg/kg dose of SAHA combined with 10 mg/kg dose of arimoclomol (SAHA+Arim.) or vehicle (Veh; 5% DMSO, 40% PEG300, 5% Tween-80, 50% Saline) through intraperitoneal injection, every three days, starting from 7 days of age. The impact of SAHA, or arimoclomol or SAHA combined with arimoclomol on protein biomarkers in Thy1-hTDP-43 mice was evaluated at disease onset (14 days of age for SAHA) or at symptomatic stage (17 days of age for SAHA, Arim. and SAHA+Arim.) through biochemical analysis. Furthermore, the impact of a 50 mg/kg dose of SAHA administered daily was assessed in Thy1-hTDP-43 mice from the age of 7 days until the age of 14 days. Mice were weighed daily, at the same time of day, on a balance with 0.1 g readability and ± 0.3 g linearity (EU-C 7500PT, Gibertini).

Statistical analyses

Prism 10.0 (GraphPad Software Inc., San Diego, CA) was used. For each variable, the differences between experimental groups were analysed by Student's t test, Mann Whitney or one-way ANOVA followed by post-hoc tests. Two-way ANOVA for repeated measure followed by Sidak's post-hoc test was used to analyse body weight of SAHA-treated and vehicle mice. P values below 0.05 were considered significant.

Results

SAHA reverses TDP-43 mislocalization and increases PPIA acetylation in an *in vitro* model

To investigate the effect of Lys-acetylation on TDP-43 proteinopathy we performed an HDACi screening on a cellular model of chronic nutrient starvation [43]. Under these conditions, HEK293 cells present cytoplasmic mislocalization of TDP-43 and its C-terminal fragment of 35 kDa (TDP-35CTF) (Fig. 1A-B). We measured the effect of a number of HDACis, i.e. SAHA, RGFP109, RGFP966, ACY-738, tubastatin A and selisistat on TDP-43 cytoplasmic mislocalization and found that only SAHA was able to restore control conditions by analyzing both full-length TDP-43 and TDP-35CTF, and this effect was dose-dependent (Fig. 1A-B and Supplementary Fig. 1A-D). Notably, ACY-738 specific HDAC6 inhibitor even increased significantly the accumulation of cytoplasmic TDP-43 (Fig. 1A). SAHA has a relatively broad specificity, but is a potent HDAC1 and HDAC3 inhibitor [48]. RGFP966 HDAC3 specific inhibitor did not reduced cytoplasmic TDP-43 accumulation, suggesting that SAHA may impact on TDP-43 trafficking mainly through an HDAC1-dependent mechanism.

We previously demonstrated that the interaction of PPIA with TDP-43 is favored by PPIAK125 acetylation [18]. We therefore evaluated the effect of SAHA on PPIA acetylation, under chronic nutrient starvation. To measure specifically PPIAK125ac we developed an antibody against a stretch of the PPIA sequence centered on the acetylated K125 (Supplementary Fig. 2). SAHA was able to significantly increase PPIAK125ac (Fig. 1C). Moreover, by knocking down experiments, we could deduce that HDAC1, and not HDAC3, deacetylates PPIAK125ac (Fig. 1D).

We conclude that SAHA is a potentially interesting candidate to mitigate TDP-43 proteinopathy possibly through PPIAK125 acetylation. We therefore further investigated the effect of SAHA on TDP-43 and PPIA acetylation in PBMCs of ALS patients and in a mouse model of TDP-43 proteinopathy.

SAHA reduces cytoplasmic TDP-43 by increasing PPIAK125ac in PBMCs of ALS patients

Previous studies detected TDP-43 mislocalization in PBMCs of ALS and ALS-FTD patients [25]. We tested whether treatment with SAHA can restore TDP-43 localization in PBMCs of ALS patients. We selected 9 ALS patients with PBMCs displaying accumulation of TDP-43 and TDP-35CTF in the cytoplasm, as detected by CEI, and low PPIAK125ac in the nucleus (Fig. 2A-E and Table 1). Two patients carried a TDP-43 mutation (TDP-43^{G295S}, TDP-43^{S393L}), but their TDP-43 distribution in PBMCs did not differ from the other sporadic patients. PBMCs from each patient were treated or not with 1 µM SAHA overnight. SAHA increased PPIAK125ac, concomitantly induced nucleus-cytoplasmic redistribution of PPIA (Fig. 2F-H) and decrease of TDP-43 and TDP-35CTF in the cytoplasm (Fig. 2I-J), without a noticeable increase in the nucleus where is already highly concentrated (data not shown). These findings further support the role of the acetylated form of PPIA in driving TDP-43 localization and the possible use of PBMCs for testing drugs targeting TDP-43 mislocalization.

Homozygous Thy1-hTDP-43 mouse is a severe model of TDP-43 proteinopathy

To test the effect of SAHA on proteinopathy *in vivo*, we used as a mouse model the homozygous Thy1-hTDP-43 mouse that develops an aggressive quadriplegia [47]. These transgenic mice overexpress 2-fold the wild-type human TDP-43 (hTDP-43) gene under the control of a murine Thy-1 promoter, which drives TDP-43 expression specifically in neurons at postnatal day 7, and show a disease onset at day 14, allowing to study *in vivo* approaches that interfere with TDP-43 proteinopathy with high reproducibility. We further reduced variability by backcrossing the original B6;SJL hybrid strain to a fully congenic C57BL/6J strain. However, these mice that express high levels of TDP-43 have a very aggressive disease and a life expectancy of less than a month, thus limiting behavioral analysis and studies on disease progression. We therefore identified a number of molecular biomarkers, as outcome measures, to evaluate the effects of drugs up to a symptomatic stage (17 days). Thy1-hTDP-43 mice show a dramatic loss of motor neurons in the spinal cord already at the onset of the disease mirrored by a great increase in plasmatic NfL (Fig. 3A-B). Neurodegeneration is accompanied by microgliosis that becomes significant respect to control at the symptomatic stage (Fig. 3C). In the spinal cord, the TDP-43 in the nucleus greatly decreases as disease progresses and accumulates in the cytoplasm, especially as TDP-35CTF, and as detergent-insoluble phosphorylated form (Fig. 3D-F). To evaluate the effects of TDP-43 pathology on splicing in the spinal cord of the Thy1-hTDP-43 mouse, we evaluated the exclusion or the inclusion respectively of a number of skiptic and cryptic exons, previously identified in mutant TDP-43 mouse models (Fig. 3G-K and Supplementary Fig. 3) [17]. All of the skiptic exons evaluated (Herc2, Ankrd42, Ube3C, Slc6a6, Plod1, Pex16, Pacrgl) were detected and the level of the exon exclusion increased as disease progresses, particularly for Ankrd42, Pacrgl, Slc6a6 and Herc2 that already at the onset were significantly

higher respect to the presymtomatic stage (Fig. 3H-K and Supplementary Fig. 3A-C). Instead, none of the cryptic exons analyzed (Adipor2, Adnp2, A230046K03Rik, 2610507B11Rik, Celf5) were detected (data not shown). PPIA essentially followed TDP-43, translocating to the cytoplasm as disease progresses possibly recruited in membrane-less assemblies and/or aggregates (Fig. 3L), while PPIAK125ac is retrieved to the nucleus, probably recruited into nuclear bodies as a response to stress (Fig. 3M) [13]. Consequently, there is a loss of PPIA in the sciatic nerve (Fig. 3N), where also high levels of pTDP-43 are detected (Fig. 3O). The sciatic nerve shows a great decrease in acetylated tubulin at the onset of the disease (Fig. 3P), suggesting an early impairment of the axonal transport [49]. In the gastrocnemius muscle of the Thy1-hTDP-43 mice, the expression of fetal *AChR* γ-subunit, which in mice is normally downregulated within the first two weeks after birth [50], substantially increases at a symptomatic stage compared to the onset (Fig. 3Q), highlighting muscle denervation, as previously observed [51].

SAHA delayed the onset of TDP-43 pathology and in combination with arimoclomol reduced neuromuscular pathology markers in the mouse model

We established optimal treatment schedule for SAHA by a pilot study in which Thy1-hTDP-43 mice were treated intraperitoneally with 50 mg/kg every day or every three days from presymptomatic stage up to 14 days of age (Supplementary Fig. 4). The less frequent treatment schedule was more effective, on the basis of lower plasmatic NfL concentration and TDP-35CTF accumulation in the cytoplasm, and therefore was chosen for the following trials (Supplementary Fig. 4C-D). We performed two studies with two independent groups of mice with the aim to establish if SAHA interfered with the first phases of the pathology and if the effect was maintained over time.

In the first study, the mice were treated up to 14 days of age (onset of the disease) and sacrificed to evaluate the effect of the treatment at a molecular level using the previously established outcome measures (Fig. 4A). Compared to vehicle-treated, SAHA-treated mice had lower NfL concentration in plasma, higher *Map*-2 expression in spinal cord and lower MMP-9 in plasma (Fig. 4B-D), indexes of a reduced neurodegeneration and neuroinflammation. TDP-43 was higher in the nucleus and TDP-35CTF accumulation was lower in the cytoplasm (Fig. 4E-F) and there was a tendency to a lower pTDP-43 aggregation (Fig. 4G). A milder TDP-43 pathology was associated with a significant decrease in the exclusion of the skiptic exons for Plod1, Pex16 and Herc2 (Fig. 4H-J), a reduction in the nuclear translocation of PPIAK125ac (Fig. 4K), that is high at the onset of the disease (Fig. 3M) and likely a marker of stress response, no reduction of nuclear PPIA and a higher level of PPIA in the cytoplasm (Fig. 4L). In periphery, possibly as a consequence of a reduced PPIA recruitment in membrane-less assemblies or aggregates, we detected an increased level of PPIA in the sciatic nerve (Fig. 4M) and decreased pTDP-43 (Fig. 4N). We also detected increased acetylated tubulin (Fig. 4O) and decreased *AChR* γ-subunit expression in the gastrocnemius (Fig. 4P), suggesting a delayed impairment in the neuromuscular function. Finally, we also checked the effect of SAHA on *Hdac1, 2, 3, 4*, and *6* mRNA expression and found that there was a significant downregulation of *Hdac1*, *2*, and *3*, likely

contributing to its potent inhibition on class I HDACs, but no effect on *Hdac4* and *6* mRNA expression, (Supplementary Fig. 5A-E).

In the second study, we treated mice with the same schedule up to 17 days of age and evaluated the effect of SAHA on the same outcome measures (Fig. 5A). In this group of mice, the body weight was monitored daily confirming the delayed onset of the disease (Fig. 5B) underlined by the low level of nuclear PPIAK125ac at 14 days of age (Fig. 4K), similarly to the presymptomatic stage (Fig. 3M). In particular, ponderal growth trajectories were significantly different from 13 days of age, when vehicle-treated mice increased weight at a slower rate than the SAHA-treated mice (Fig. 5B). There was a reduced NfL concentration in plasma (Fig. 5C), however the effect on most of the other biomarkers was lost with the longer treatment (Fig. 5D-Q). There was even a tendency to an increased TDP-43 proteinopathy, no decrease of TDP-43 in the nucleus, but a significant accumulation of TDP-43 in the cytoplasm (Fig. 5F), a tendency to an increase in pTDP-43 aggregation (Fig. 5H) and no improvement in the TDP-43 splicing function (Fig. 5I-K). There was no change in the level of nuclear PPIAK125ac (Fig. 5L), a decrease of PPIA in the cytoplasm with only a tendency to increase in the nucleus (Fig. 5M), likely indicating its extracellular secretion in response to the persistent cellular stress [52]. Moreover, there was a decrease in the mRNA expression of *Hdac4* and *Hdac6*, not detected in the first shorter study (Supplementary Fig. 5I-J). HDAC4 plays an important role in protecting the neuromuscular function in ALS [34,35], while HDAC6 is involved in the clearance of misfolded proteins [53,54]. This may suggest that longer SAHA treatment could not be effective also because of an accumulation of a number of undesirable side effects.

In vitro studies in ALS models have reported that SAHA may act as an HSP co-inducer and that this effect is potentiated by arimoclomol. We therefore tested if the combination of the two drugs were more effective in Thy1-hTDP-43 mice in counteracting the 2-fold hTDP-43 overexpression and compensate for the side effects. We treated mice with SAHA+arimoclomol, with the same schedule up to 17 days of age, and evaluated the effect of the treatment on the outcome measures (Fig. 6). The treatment increased HSP70 level in the spinal cord and respect to SAHA alone had a stronger neuroprotective effect (Fig. 5C), with a greater decrease in NfL (-25% with SAHA versus -38% with SAHA+arimoclomol), and a significant decrease of MMP-9 in plasma (Fig. 6B,C,E). Although TDP-43 pathology in the spinal cord did not greatly improve, no worsening was observed (Fig. 6F-H), as seen with SAHA alone (Fig. 5F-H), and an improvement in the TDP-43 splicing function was detected, with a significant decrease in the exclusion of the skiptic exons for Ube3C, and Slc6a6 (Fig. 6I-J). No significant accumulation of cytoplasmic TDP-43 compared to vehicle-treated mice (Fig. 6F versus Fig. 5F) and no significant decrease in cytoplasmic PPIA were observed (Fig. 6L versus Fig. 5M). Moreover, SAHA+arimoclomol did not affect *Hdac4* and *Hdac6* mRNA expression (Supplementary Fig. 5N-O), indicating that possible negative effects from *Hdac4* and *Hdac6* downregulation were rescued. Interestingly, a great improvement was seen in periphery, regardless no change in PPIA (Fig. 6M). Mice treated with the combination showed a substantial increase in acetylated tubulin, an equally important decrease in pTDP-43 in the sciatic nerve and a significant decrease in the *AChR* γ-subunit expression in the gastrocnemius muscle (Fig. 6N-P). Arimoclomol alone was not affecting acetylation of tubulin, suggesting a possible

synergistic effect of the two drugs on HDAC6 inhibition (Supplementary Fig. 6B). Moreover, arimoclomol did not reduce pTDP-43 levels in the sciatic nerve, nor did it affect pTDP-43 aggregation in the spinal cord, as the combination (Supplementary Fig. 6C-D). It reduced NfL and *AChR* γ-subunit expression, although not to the same extent as the combination (Supplementary Fig. 6E-F). Overall, arimoclomol potentiated the positive effects of SAHA in periphery and mitigated its side effects.

Discussion

HDACis are valuable tools to explore acetylation homeostasis and hold potential for treating neurodegeneration, but they have been scarcely investigated in the context of TDP-43 pathology. Several of them are in advanced stages of development or have been approved for cancer therapy, such as SAHA, therefore they might be suitable candidates for repurposing. However, it is important to emphasize that HDACis are potent drugs that induce extensive transcriptional changes and should therefore be carefully studied in the specific disease models throughout the progression of the disease to derive the net effect of their multiple actions.

Our interest in HDACis stems from the observation that Lys-acetylation is involved in the interaction of TDP-43 with PPIA, which has a key role in regulating TDP-43 localization and function [15,16,46]. In this work we found that HDAC1 is responsible for PPIA deacetylation and that, inhibiting this pathway by SAHA, TDP-43 proteinopathy is reduced in a cellular model of chronic nutrient starvation and in PBMCs of ALS patients. SAHA also delayed the onset of TDP-43 pathology in an aggressive mouse model of TDP-43 proteinopathy, but the effect was temporary. When in combination with the HSP co-inducer arimoclomol a mitigation of the neurodegeneration was maintained over time. Moreover, there was a great reduction of the pathological markers in the sciatic nerve, including pTDP-43, and markers of axonal stability and muscle denervation.

HDAC inhibition have been largely investigated in preclinical trials with several mouse model of ALS [31], but never with a mouse model of TDP-43 proteinopathy. However, indications of possible positive effects were reported *in vitro* in mutant TDP-43 iPSC-derived spinal motor neurons where an HDAC6 inhibitor rescued TDP-43 pathology and axonal transport defects [15]. Our purpose was to investigate the impact of acetylation homeostasis in the early steps driving TDP-43 pathology, which likely lead to nucleocytoplasmic transport impairment and clearance of nuclear TDP-43 that are associated with TDP-43 dysfunction in a wide range of aspects of RNA metabolism. In the *in vitro* screening, SAHA turned out to be the most effective in inhibiting accumulation of TDP-43 and TDP-35CTF in the cytoplasm. SAHA is considered a broad-spectrum inhibitor since can inhibit HDAC1 and HDAC3 class I enzymes, but also the HDAC6 class II enzyme, although less efficiently [55–58]. However, in our assay, the absence of an effect of HDAC6 and HDAC3 specific inhibitors point to an involvement of an HDAC1-dependent mechanism. In addition, our siRNA experiments indicate that PPIA is deacetylated by HDAC1, as also suggested by an interactomic study [23]. Moreover, HDCA1 reduction and inhibition was protective against mutant TDP-43 toxicity [59]. The effect of SAHA on TDP-43 localization was also confirmed in ALS patient PBMCs. These cells have shown to display

cytoplasmic accumulation of TDP-43 in a previous study [25]. In a later study, we have also shown that, in PBMCs from a relative large cohort of ALS patients, TDP-43 was entrapped in supramolecular assemblies with hnRNPA2B1 and PPIA [26]. Altogether, these findings suggest that PBMCs may be useful to test the effect of therapeutic approaches targeting TDP-43 proteinopathy in patients and possible monitor clinical trials.

To test the effect of SAHA on the onset of TDP-43 proteinopathy *in vivo,* we chose a model with marked pathology induced in neurons by hTDP-43 overexpression, in absence of a specific mutation. The mice show neuromuscular junction (NMJ) pathology, denervation of distal muscles and motor neuron loss, as observed in ALS patients [47,60]. Moreover, the timing of the onset of the proteinopathy is well defined and, because of the short life span, preclinical studies with multiple treatment schedules and drug combinations are feasible. However, due to the neonatal onset and severity of the disease, behavioral studies on disease progression are limited. Therefore, we performed multiple molecular evaluations at different stages of the disease to identify surrogate markers. Interestingly, we could monitor TDP-43 impairment in splicing function with the progression of the disease and in response to SAHA treatment. In particular, we evaluated known skiptic exons, i.e. excision of otherwise normally conserved exons, and cryptic exons, i.e. decreased excision of non-conserved cryptic exons, that are the result of TDP-43 dysfunction [17,61]. We could demonstrate that in conditions of transgenic overexpression of the hTDP-43 protein, there is no loss of the TDP-43 cryptic exon excision function, while increased exon skipping can be seen already at an early stage of the disease and seems to be a good proxy of nuclear TDP-43 levels. It has been hypothesized that exclusion of highly conserved skiptic exons in an early phase may affect key cellular pathways such as protein degradation (Ube3C, Herc2, Pacrgl) and inflammatory response (Ankrd42) that in turn could drive TDP-43 aggregation, nuclear depletion and loss of TDP-43 function [17,62]. In a second phase, this may lead to increasing occurrence of cryptic exons, which possibly are not observable in a mouse model with such a fast disease progression.

In PBMCs of ALS patients we could correlate reduced TDP-43 proteinopathy with increased nuclear PPIAK125ac due to lysine deacetylation inhibition with SAHA. In the mice this effect could be also associated with an improved splicing function of TDP-43 only in the short-term study. Instead, with the longer treatment the positive effects were mitigated, possibly because SAHA has an impact especially on TDP-43 trafficking at the onset of TDP-43 proteinopathy. However, over-time, its effect is insufficient to counteract the 2-fold overexpression of hTDP-43 in the neurons of Thy1-hTDP-43 mice. Moreover, with the longer treatment, the broad-spectrum HDAC inhibition by SAHA may induce side effects specifically in the nervous system. We found downregulation of HDAC4 and HDAC6. Other studies reported an inhibitory effect of SAHA on HDAC4 [63], which has an essential role in synaptic plasticity and memory formation [64], and in compensatory muscle reinnervation during ALS [35]. SAHA inhibits also HDAC6, although not greatly (IC_{50} >30 nM) [55–58]. Its inhibition favors axonal transport [15] and axonal outgrowth [65], but at the same time may increase TDP-43 acetylation, a determinant of TDP-43 aggregate formation [66]. The latest aspect is particularly critical in a condition of high susceptibility to TDP-43 proteinopathy and TDP-43 overexpression. An indication of a possible negative effect of HDAC6 inhibition on TDP-43 mislocalization, was also obtained in our experiments *in vitro* with specific HDAC6 inhibitors.

To overcome overexpression and consequent aggregation of TDP-43 in the mouse model, we tested the SAHA+arimoclomol combination. Arimoclomol is a small drug that prolongs the activation and the DNA binding of the HSF-1 transcription factor, upregulating the molecular chaperone family of HSPs (i.e. Hsp70, Hsp90). Although arimoclomol was effective at ameliorating disease phenotypes in multiple preclinical models of motor neuron disease [67–69], it failed to modify the progression of the disease in a phase 3 clinical trial for ALS [70]. The combination SAHA+arimoclomol is known to have a synergistic effect in enhancing stress-induced Hsp70 expression in spinal cord-dorsal root ganglion cultures in response to proteotoxic stress [40]. Moreover, RGFP963, another class I HDACi, in combination with arimoclomol significantly increased axonal transport in cultures expressing mutant SOD1 [41]. The mechanisms by which HDAC inhibition and HSP co-inducers interact and enhance HSP response is complex and not fully elucidated. While HDAC inhibitors have shown HSP-inducing properties, HDAC inhibitory activity of arimoclomol was only hypothesized [40]. In this work, we provided evidence *in vivo* that the combination boosted neuroaxonal and neuromuscular protection, without full recovery from TDP-43 proteinopathy and only a partial rescue of the splicing function. The combination SAHA+arimoclomol was more effective in decreasing markers of neurodegeneration and neuroinflammation (NfL, MMP-9), but especially greatly reduced markers of neuromuscular pathology in sciatic nerve and gastrocnemius muscle: tubulin deacetylation, accumulation of pTDP-43 and AChR γ-subunit re-expression. Acetylation of α-tubulin at Lys-40 is a marker of microtubule stability and promotes the recruitment of the molecular motors dynein and kinesin-1 to microtubules, promoting anterograde and retrograde transport [71]. In fact, increasing tubulin acetylation through HDAC6 inhibition has improved axonal transport in models of ALS and Charcot-Marie-Tooth Disease [72,73]. This in turn may favor axonal transport of TDP-43 mRNP granules and facilitate delivery of TDP-43 mRNA targets to distal neuronal compartments [74], thus explaining the reduction of pTDP-43 accumulation in the sciatic nerve. Previous studies have shown that NMJ innervation of muscles was better preserved by either HDAC6 inhibition or arimoclomol treatment individually [67,73]. In the fetal AChR isoform of skeletal muscle endplates, the γ-subunit is downregulated after birth and replaced by the ε-subunit, except in cases of denervation, where the fetal form is re-expressed in the muscle. Indeed, downregulation of the γ-subunit has been detected in ALS mice following treatments that preserve innervation and muscle mass in the hindlimbs [75,76]. Here, in the longer treatment, we observed only a tendency to decrease in AChR γ-subunit expression following treatment with either SAHA or arimoclomol individually, while the effect was significant when the two were used in combination. This result is particularly notable given that Thy1-hTDP-43 mice exhibit pronounced NMJ denervation in hindlimb muscles and NMJ pathology is restricted to motor nerve terminals [60].

There is an increasing interest in testing drug cocktails, especially with repurposed drug candidates, because of the multifactorial nature of ALS. Our results highlight the importance of *in vivo* investigations for addressing the complexity of drug mechanisms, especially in combination therapies, to reveal unpredictable negative or positive effects of drug-drug interaction in specific tissues/organs and stages of the disease, which may be overlooked in cell culture studies. It would be interesting to evaluate the effect of a selective HDAC1

inhibitor, in combination or not with arimoclomol, to increase more specifically PPIA acetylation and reduce side effects derived by broad HDAC inhibition. Although the Thy1-hTDP-43 mouse is useful to decipher early molecular mechanisms at the basis of TDP-43 proteinopathy and NMJ denervation, has an excessively aggressive disease and is limited in evaluating the effects of drugs with the progression of the disease. Experiments with a mouse model with a slower and adult onset disease are warranted.

Regarding the role of PPIA, these studies further suggest that TDP-43 localization and function is critically influenced by PPIA. Its acetylation on K125 is able to reverse TDP-43 localization in a cellular model of TDP-43 proteinopathy and in PBMCs of ALS patients, where TDP-43 likely undergoes liquid demixing, but does not irreversibly aggregate. From the studies in mice, it appeared that PPIA125Kac is involved in an early response that neurons adopt to counteract TDP-43 altered homeostasis. It is possible that PPIA and its acetylated form accumulate with TDP-43 in membrane-less compartments in response to stress, as reported in other paradigms [11,12,20,21], and that persistent stress may lead to irreversible protein aggregation, stress-induced PPIA secretion and finally loss of a key intracellular protective factor. In fact, we previously demonstrated high PPIA in CSF and plasma of patients and animal models, low intracellular soluble PPIA and high detergent-insoluble protein in CNS tissues of ALS mouse models and ALS/FTD patients [19,24,26,52].

In conclusion, the present study suggests that HDAC inhibition, by increasing acetylated PPIA, could be beneficial for restoring TDP-43 localization and function. SAHA, a broad-range HDAC inhibitor capable of increasing PPIA acetylation, reduced TDP-43 proteinopathy in a severe and fast progressing TDP-43 overexpressing mouse model, although temporarily. Arimoclomol in combination with SAHA, mitigated side effects and showed a synergistic action in periphery, significantly reducing markers of peripheral nerve pathology and muscle denervation. Therefore, it is worthwhile to further explore lysine deacetylation inhibition and HSP induction in combination, as a potential therapeutic approach for patients.

Abbreviations

ALS: Amyotrophic lateral sclerosis: TDP-43: TAR DNA-binding protein 43 kDa; PPIA: Cyclophilin A/ Peptidyl-prolyl cis-trans isomerase A; PBMCs: peripheral blood mononuclear cells; NfL: neurofilament light chain; HSP: heat shock protein; AChR: acetylcholine receptor; FTD: frontotemporal dementia; AD: Alzheimer's disease; HDACs: histone deacetylases; HDACis: HDAC inhibitors; SAHA: suberoylanilide hydroxamic acid; WB: Western Blot; CEI: Capillary electrophoresis immunoassay; PPIAK125ac: K125 acetylated PPIA; MMP-9: matrix metalloproteinase-9; TDP-35CTF: C-terminal fragment of 35 kDa.

Declarations

Ethical approval and consent to participate

Subjects enrolled in this study signed a written informed consent before blood drawn. The study was supported by the Italian Ministry of Health and approved by the Ethics Committee of the Azienda Ospedaliero-Universitaria Città della Salute e della Scienza di Torino (protocol number 0062147 June 19, 2019), in accordance with the ethical standards laid down in the 1964 Declaration of Helsinki and its later amendments.

Consent for publication

All authors have given their consent for publication.

Availability of supporting data

Data that support the findings of this study are available within the paper and Supplementary material. Raw data have been deposited in the Zenodo public repository (https://zenodo.org/).

Competing interests

No competing interests

Funding

This project received funding from the Italian Ministry of Health (RF-2018-12365614).

Authors's contributions

VB and LP were responsible for conception and design of the study. All authors contributed to data acquisition and analysis. VB and LP contributed to drafting the text and preparing the figures. All authors critically evaluated and approved the final manuscript.

Acknowledgements

We would like to express our sincere gratitude to the patients who generously agreed to participate in this study.

Authors' information

Laura Pasetto and Valentina Bonetto are co-corresponding authors

Affiliations

Istituto di Ricerche Farmacologiche Mario Negri IRCCS, Milano (Italy)

Serena Scozzari, Stefano Fabrizio Columbro, Monica Favagrossa, Massimo Tortarolo, Alfredo Cagnotto, Mario Salmona, Caterina Bendotti, Laura Pasetto, Valentina Bonetto

'Rita Levi Montalcini' Department of Neuroscience, Università degli Studi di Torino, Torino, Italy

Giovanni De Marco, Andrea Calvo

Corresponding authors

Correspondence should be addressed to Laura Pasetto (laura.paetto@marionegri.it) or Valentina Bonetto (valentina.bonetto@marionegri.it)

References

1. Neumann M, Sampathu DM, Kwong LK, Truax AC, Micsenyi MC, Chou TT, et al. Ubiquitinated TDP-43 in frontotemporal lobar degeneration and amyotrophic lateral sclerosis. Science. 2006;314:130–3.

2. McAleese KE, Walker L, Erskine D, Thomas AJ, McKeith IG, Attems J. TDP-43 pathology in Alzheimer's disease, dementia with Lewy bodies and ageing. Brain Pathol. 2017;27:472–9.

3. Nelson PT, Dickson DW, Trojanowski JQ, Jack CR, Boyle PA, Arfanakis K, et al. Limbic-predominant age-related TDP-43 encephalopathy (LATE): consensus working group report. Brain. 2019;142:1503–27.

4. Nicks R, Clement NF, Alvarez VE, Tripodis Y, Baucom ZH, Huber BR, et al. Repetitive head impacts and chronic traumatic encephalopathy are associated with TDP-43 inclusions and hippocampal sclerosis. Acta Neuropathol (Berl). 2023;145:395–408.

5. Yamashita R, Beck G, Yonenobu Y, Inoue K, Mitsutake A, Ishiura H, et al. TDP-43 Proteinopathy Presenting with Typical Symptoms of Parkinson's Disease. Mov Disord Off J Mov Disord Soc. 2022;37:1561–3.

6. Sanchez II, Nguyen TB, England WE, Lim RG, Vu AQ, Miramontes R, et al. Huntington's disease mice and human brain tissue exhibit increased G3BP1 granules and TDP43 mislocalization. J Clin Invest. 2021;131:e140723, 140723.

7. de Boer EMJ, Orie VK, Williams T, Baker MR, De Oliveira HM, Polvikoski T, et al. TDP-43 proteinopathies: a new wave of neurodegenerative diseases. J Neurol Neurosurg Psychiatry. 2020;

8. Ratti A, Buratti E. Physiological functions and pathobiology of TDP-43 and FUS/TLS proteins. J Neurochem. 2016;138 Suppl 1:95–111.

9. Ayala YM, De Conti L, Avendaño-Vázquez SE, Dhir A, Romano M, D'Ambrogio A, et al. TDP-43 regulates its mRNA levels through a negative feedback loop. EMBO J. 2011;30:277–88.

10. Polymenidou M, Lagier-Tourenne C, Hutt KR, Huelga SC, Moran J, Liang TY, et al. Long pre-mRNA depletion and RNA missplicing contribute to neuronal vulnerability from loss of TDP-43. Nat Neurosci. 2011;14:459–68.

11. Yu H, Lu S, Gasior K, Singh D, Vazquez-Sanchez S, Tapia O, et al. HSP70 chaperones RNA-free TDP-43 into anisotropic intranuclear liquid spherical shells. Science. 2021;371:eabb4309.

12. Lu S, Hu J, Arogundade OA, Goginashvili A, Vazquez-Sanchez S, Diedrich JK, et al. Heat-shock chaperone HSPB1 regulates cytoplasmic TDP-43 phase separation and liquid-to-gel transition. Nat Cell Biol. 2022;24:1378–93.

13. Wang C, Duan Y, Duan G, Wang Q, Zhang K, Deng X, et al. Stress Induces Dynamic, Cytotoxicity-Antagonizing TDP-43 Nuclear Bodies via Paraspeckle LncRNA NEAT1-Mediated Liquid-Liquid Phase Separation. Mol Cell. 2020;79:443-458.e7.

14. Gasset-Rosa F, Lu S, Yu H, Chen C, Melamed Z, Guo L, et al. Cytoplasmic TDP-43 De-mixing Independent of Stress Granules Drives Inhibition of Nuclear Import, Loss of Nuclear TDP-43, and Cell Death. Neuron. 2019;102:339-357.e7.

15. Fazal R, Boeynaems S, Swijsen A, De Decker M, Fumagalli L, Moisse M, et al. HDAC6 inhibition restores TDP-43 pathology and axonal transport defects in human motor neurons with TARDBP mutations. EMBO J. 2021;40:e106177.

16. Chou C-C, Zhang Y, Umoh ME, Vaughan SW, Lorenzini I, Liu F, et al. TDP-43 pathology disrupts nuclear pore complexes and nucleocytoplasmic transport in ALS/FTD. Nat Neurosci. 2018;21:228–39.

17. Fratta P, Sivakumar P, Humphrey J, Lo K, Ricketts T, Oliveira H, et al. Mice with endogenous TDP-43 mutations exhibit gain of splicing function and characteristics of amyotrophic lateral sclerosis. EMBO J. 2018;37.

18. Lauranzano E, Pozzi S, Pasetto L, Stucchi R, Massignan T, Paolella K, et al. Peptidylprolyl isomerase A governs TARDBP function and assembly in heterogeneous nuclear ribonucleoprotein complexes. Brain. 2015;138:974–91.

19. Pasetto L, Grassano M, Pozzi S, Luotti S, Sammali E, Migazzi A, et al. Defective cyclophilin A induces TDP-43 proteinopathy: implications for amyotrophic lateral sclerosis and frontotemporal dementia. Brain. 2021;144:3710–26.

20. Curdy N, Lanvin O, Cerapio J-P, Pont F, Tosolini M, Sarot E, et al. The proteome and transcriptome of stress granules and P bodies during human T lymphocyte activation. Cell Rep. 2023;42:112211.

21. Xiang S, Kato M, Wu LC, Lin Y, Ding M, Zhang Y, et al. The LC Domain of hnRNPA2 Adopts Similar Conformations in Hydrogel Polymers, Liquid-like Droplets, and Nuclei. Cell. 2015;163:829–39.

22. Babu M, Favretto F, Rankovic M, Zweckstetter M. Peptidyl Prolyl Isomerase A Modulates the Liquid–Liquid Phase Separation of Proline-Rich IDPs. J Am Chem Soc. 2022;144:16157–63.

23. Maneix L, Iakova P, Lee CG, Moree SE, Lu X, Datar GK, et al. Cyclophilin A supports translation of intrinsically disordered proteins and affects haematopoietic stem cell ageing. Nat Cell Biol. 2024;26:593–603.

24. Basso M, Samengo G, Nardo G, Massignan T, D'Alessandro G, Tartari S, et al. Characterization of detergent-insoluble proteins in ALS indicates a causal link between nitrative stress and aggregation in pathogenesis. PLoS One. 2009;4:e8130.

25. De Marco G, Lupino E, Calvo A, Moglia C, Buccinna B, Grifoni S, et al. Cytoplasmic accumulation of TDP-43 in circulating lymphomonocytes of ALS patients with and without TARDBP mutations. Acta Neuropathol. 2011;121:611–22.

26. Luotti S, Pasetto L, Porcu L, Torri V, Elezgarai SR, Pantalone S, et al. Diagnostic and prognostic values of PBMC proteins in amyotrophic lateral sclerosis. Neurobiol Dis. 2020;139:104815.

27. Choudhary C, Kumar C, Gnad F, Nielsen ML, Rehman M, Walther TC, et al. Lysine acetylation targets protein complexes and co-regulates major cellular functions. Science. 2009;325:834–40.

28. Saha RN, Pahan K. HATs and HDACs in neurodegeneration: a tale of disconcerted acetylation homeostasis. Cell Death Differ. 2006;13:539–50.

29. Narita T, Weinert BT, Choudhary C. Functions and mechanisms of non-histone protein acetylation. Nat Rev Mol Cell Biol. 2019;20:156–74.

30. Shukla S, Tekwani BL. Histone Deacetylases Inhibitors in Neurodegenerative Diseases, Neuroprotection and Neuronal Differentiation. Front Pharmacol. 2020;11:537.

31. Klingl YE, Pakravan D, Van Den Bosch L. Opportunities for histone deacetylase inhibition in amyotrophic lateral sclerosis. Br J Pharmacol. 2021;178:1353–72.

32. Piepers S, Veldink JH, de Jong SW, van der Tweel I, van der Pol W-L, Uijtendaal EV, et al. Randomized sequential trial of valproic acid in amyotrophic lateral sclerosis. Ann Neurol. 2009;66:227–34.

33. Cudkowicz ME, Andres PL, Macdonald SA, Bedlack RS, Choudry R, Brown RH, et al. Phase 2 study of sodium phenylbutyrate in ALS. Amyotroph Lateral Scler Off Publ World Fed Neurol Res Group Mot Neuron Dis. 2009;10:99–106.

34. Boutillier A-L, Tzeplaeff L, Dupuis L. The dark side of HDAC inhibition in ALS. EBioMedicine. 2019;41:38–9.

35. Pigna E, Simonazzi E, Sanna K, Bernadzki KM, Proszynski T, Heil C, et al. Histone deacetylase 4 protects from denervation and skeletal muscle atrophy in a murine model of amyotrophic lateral sclerosis. EBioMedicine. 2019;40:717–32.

36. Davis N, Taylor B, Abelleira-Hervas L, Karimian-Marnani N, Aleksynas R, Syed N, et al. Histone deacetylase-3 regulates the expression of the amyloid precursor protein and its inhibition promotes neuroregenerative pathways in Alzheimer's disease models. FASEB J Off Publ Fed Am Soc Exp Biol. 2024;38:e23659.

37. Guo W, Naujock M, Fumagalli L, Vandoorne T, Baatsen P, Boon R, et al. HDAC6 inhibition reverses axonal transport defects in motor neurons derived from FUS-ALS patients. Nat Commun. 2017;8:861.

38. Rossaert E, Pollari E, Jaspers T, Van Helleputte L, Jarpe M, Van Damme P, et al. Restoration of histone acetylation ameliorates disease and metabolic abnormalities in a FUS mouse model. Acta Neuropathol Commun. 2019;7:107.

39. Valle C, Salvatori I, Gerbino V, Rossi S, Palamiuc L, René F, et al. Tissue-specific deregulation of selected HDACs characterizes ALS progression in mouse models: pharmacological characterization of SIRT1 and SIRT2 pathways. Cell Death Dis. 2014;5:e1296.

40. Kuta R, Larochelle N, Fernandez M, Pal A, Minotti S, Tibshirani M, et al. Depending on the stress, histone deacetylase inhibitors act as heat shock protein co-inducers in motor neurons and potentiate arimoclomol, exerting neuroprotection through multiple mechanisms in ALS models. Cell Stress Chaperones. 2020;25:173–91.

41. Fernández Comaduran M, Minotti S, Jacob-Tomas S, Rizwan J, Larochelle N, Robitaille R, et al. Impact of histone deacetylase inhibition and arimoclomol on heat shock protein expression and disease biomarkers in primary culture models of familial ALS. Cell Stress Chaperones. 2024;29:359–80.

42. Fourier A, Escal J, Bernard E, Lachman I, Perret-Liaudet A, Leblanc P, et al. Development of an automated capillary nano-immunoassay-Simple Western assay-to quantify total TDP43 protein in human platelet samples. Anal Bioanal Chem. 2019;411:267–75.

43. Reineke LC, Cheema SA, Dubrulle J, Neilson JR. Chronic starvation induces noncanonical pro-death stress granules. J Cell Sci. 2018;131.

44. Miskolci V, Hodgson L, Cox D, Vancurova I. Western analysis of intracellular interleukin-8 in human mononuclear leukocytes. Methods Mol Biol Clifton NJ. 2014;1172:285–93.

45. Tortarolo M, Vallarola A, Lidonnici D, Battaglia E, Gensano F, Spaltro G, et al. Lack of TNF-alpha receptor type 2 protects motor neurons in a cellular model of amyotrophic lateral sclerosis and in mutant SOD1 mice but does not affect disease progression. J Neurochem [Internet]. 2015; Available from: http://www.ncbi.nlm.nih.gov/pubmed/25940956

46. Kowalczyk W, Monsó M, de la Torre BG, Andreu D. Synthesis of multiple antigenic peptides (MAPs)-strategies and limitations. J Pept Sci Off Publ Eur Pept Soc. 2011;17:247–51.

47. Wils H, Kleinberger G, Janssens J, Pereson S, Joris G, Cuijt I, et al. TDP-43 transgenic mice develop spastic paralysis and neuronal inclusions characteristic of ALS and frontotemporal lobar degeneration. Proc Natl Acad Sci U S A. 2010;107:3858–63.

48. El-Awady R, Saleh E, Hamoudi R, Ramadan WS, Mazitschek R, Nael MA, et al. Discovery of novel class of histone deacetylase inhibitors as potential anticancer agents. Bioorg Med Chem. 2021;42:116251.

49. d'Ydewalle C, Krishnan J, Chiheb DM, Van Damme P, Irobi J, Kozikowski AP, et al. HDAC6 inhibitors reverse axonal loss in a mouse model of mutant HSPB1–induced Charcot-Marie-Tooth disease. Nat Med. 2011;17:968–74.

50. Missias AC, Chu GC, Klocke BJ, Sanes JR, Merlie JP. Maturation of the acetylcholine receptor in skeletal muscle: regulation of the AChR gamma-to-epsilon switch. Dev Biol. 1996;179:223–38.

51. Margotta C, Fabbrizio P, Ceccanti M, Cambieri C, Ruffolo G, D'Agostino J, et al. Immune-mediated myogenesis and acetylcholine receptor clustering promote a slow disease progression in ALS mouse models. Inflamm Regen. 2023;43:19.

52. Pasetto L, Pozzi S, Castelnovo M, Basso M, Estevez AG, Fumagalli S, et al. Targeting Extracellular Cyclophilin A Reduces Neuroinflammation and Extends Survival in a Mouse Model of Amyotrophic Lateral Sclerosis. J Neurosci Off J Soc Neurosci. 2017;37:1413–27.

53. Lee JY, Koga H, Kawaguchi Y, Tang W, Wong E, Gao YS, et al. HDAC6 controls autophagosome maturation essential for ubiquitin-selective quality-control autophagy. EMBO J. 2010;29:969–80.

54. Kawaguchi Y, Kovacs JJ, McLaurin A, Vance JM, Ito A, Yao TP. The deacetylase HDAC6 regulates aggresome formation and cell viability in response to misfolded protein stress. Cell. 2003;115:727–38.

55. Witter DJ, Harrington P, Wilson KJ, Chenard M, Fleming JC, Haines B, et al. Optimization of biaryl Selective HDAC1&2 Inhibitors (SHI-1:2). Bioorg Med Chem Lett. 2008;18:726–31.

56. Padige G, Negmeldin AT, Pflum MKH. Development of an ELISA-Based HDAC Activity Assay for Characterization of Isoform-Selective Inhibitors. SLAS Discov. 2015;20:1277–85.

57. Jones P, Altamura S, De Francesco R, Gallinari P, Lahm A, Neddermann P, et al. Probing the elusive catalytic activity of vertebrate class IIa histone deacetylases. Bioorg Med Chem Lett. 2008;18:1814–9.

58. Huber K, Doyon G, Plaks J, Fyne E, Mellors JW, Sluis-Cremer N. Inhibitors of Histone Deacetylases. J Biol Chem. 2011;286:22211–8.

59. Sanna S, Esposito S, Masala A, Sini P, Nieddu G, Galioto M, et al. HDAC1 inhibition ameliorates TDP-43-induced cell death in vitro and in vivo. Cell Death Dis. 2020;11:369.

60. Alhindi A, Shand M, Smith HL, Leite AS, Huang Y-T, van der Hoorn D, et al. Neuromuscular junction denervation and terminal Schwann cell loss in the hTDP-43 overexpression mouse model of amyotrophic lateral sclerosis. Neuropathol Appl Neurobiol. 2023;49:e12925.

61. Ling JP, Pletnikova O, Troncoso JC, Wong PC. TDP-43 repression of nonconserved cryptic exons is compromised in ALS-FTD. Science. 2015;349:650–5.

62. Rouaux C, Gonzalez De Aguilar J, Dupuis L. Unmasking the skiptic task of TDP-43. EMBO J. 2018;37:e99645.

63. Ho TCS, Chan AHY, Ganesan A. Thirty Years of HDAC Inhibitors: 2020 Insight and Hindsight. J Med Chem. 2020;63:12460–84.

64. Kim M-S, Akhtar MW, Adachi M, Mahgoub M, Bassel-Duby R, Kavalali ET, et al. An Essential Role for Histone Deacetylase 4 in Synaptic Plasticity and Memory Formation. J Neurosci. 2012;32:10879–86.

65. Kalinski AL, Kar AN, Craver J, Tosolini AP, Sleigh JN, Lee SJ, et al. Deacetylation of Miro1 by HDAC6 blocks mitochondrial transport and mediates axon growth inhibition. J Cell Biol. 2019;218:1871–90.

66. Cohen TJ, Hwang AW, Restrepo CR, Yuan C-X, Trojanowski JQ, Lee VMY. An acetylation switch controls TDP-43 function and aggregation propensity. Nat Commun. 2015;6:5845.

67. Kieran D, Kalmar B, Dick JR, Riddoch-Contreras J, Burnstock G, Greensmith L. Treatment with arimoclomol, a coinducer of heat shock proteins, delays disease progression in ALS mice. Nat Med. 2004;10:402–5.

68. Kalmar B, Novoselov S, Gray A, Cheetham ME, Margulis B, Greensmith L. Late stage treatment with arimoclomol delays disease progression and prevents protein aggregation in the SOD1 mouse model of ALS. J Neurochem. 2008;107:339–50.

69. Ahmed M, Spicer C, Harley J, Taylor JP, Hanna M, Patani R, et al. Amplifying the Heat Shock Response Ameliorates ALS and FTD Pathology in Mouse and Human Models. Mol Neurobiol. 2023;60:6896–915.

70. Benatar M, Hansen T, Rom D, Geist MA, Blaettler T, Camu W, et al. Safety and efficacy of arimoclomol in patients with early amyotrophic lateral sclerosis (ORARIALS-01): a randomised, double-blind, placebo-controlled, multicentre, phase 3 trial. Lancet Neurol. 2024;23:687–99.

71. Dompierre JP, Godin JD, Charrin BC, Cordelières FP, King SJ, Humbert S, et al. Histone deacetylase 6 inhibition compensates for the transport deficit in Huntington's disease by increasing tubulin acetylation. J Neurosci Off J Soc Neurosci. 2007;27:3571–83.

72. d'Ydewalle C, Benoy V, Van Den Bosch L. Charcot-Marie-Tooth disease: Emerging mechanisms and therapies. Int J Biochem Cell Biol. 2012;44:1299–304.

73. Taes I, Timmers M, Hersmus N, Bento-Abreu A, Van Den Bosch L, Van Damme P, et al. Hdac6 deletion delays disease progression in the SOD1G93A mouse model of ALS. Hum Mol Genet. 2013;22:1783–90.

74. Alami NH, Smith RB, Carrasco MA, Williams LA, Winborn CS, Han SS, et al. Axonal Transport of TDP-43 mRNA Granules Is Impaired by ALS-Causing Mutations. Neuron. 2014;81:536–43.

75. Trolese MC, Scarpa C, Melfi V, Fabbrizio P, Sironi F, Rossi M, et al. Boosting the peripheral immune response in the skeletal muscles improved motor function in ALS transgenic mice. Mol Ther J Am Soc Gene Ther. 2022;30:2760–84.

76. Fabbrizio P, D'Agostino J, Margotta C, Mella G, Panini N, Pasetto L, et al. Contingent intramuscular boosting of P2XR7 axis improves motor function in transgenic ALS mice. Cell Mol Life Sci. 2022;79:7.

Table 1. Demographic and clinical characteristics of ALS patients and controls

Parameters	**Healthy (n=54)**	**ALS (n=9)**
Age at sampling (years, median ± SD)	61 ± 11	65 ± 11.9
Sex (female/male)	25/29	4/5
Site of disease onset (Bulbar/Spinal)	-	0/9
ALSFRS-R at sampling (median ± SD)	-	29 ± 9.3
ΔALSFRS-R[1] (median ± SD)	-	2.3 ± 1.6
Symptom duration[2] (months, median ± SD)	-	8.0 ± 19.2
NfL (pg/ml, median ± SD)	6.7 ± 3.4	25.5 ± 10.5

[1]ΔALSFRS-R: 48–ALSFRS-R score at sampling/time from symptom onset to sampling.
[2]Symptom duration: time from symptom onset to sampling.

Figure Legends

Figure 1. SAHA reduces TDP-43 proteinopathy and increases acetyl-PPIA in an *in vitro* model. Cytoplasmic (Cyt.) levels of TDP-43 (**A**) and TDP-35CTF (**B**) in control (Ctrl; n ≥ 6) and serum-deprived HEK293 cells (Starvation), untreated (Untr; n ≥ 6) or treated with 1 μM HDACi (n=3-6): SAHA, RGF109, RGFP966, ACY-738, tubastatin A (tubA) and selisistat. Dashed line indicates Ctrl level. (**C**) PPIAK125ac levels in total lysate of control (Ctrl; n=5) and serum-deprived HEK293 cells (Starvation), untreated (Untr; n=5) or treated with 1 μM SAHA (n=6). (**D**) PPIAK125ac levels in total lysate of HEK293 transiently transfected with siRNA control (Scramble; n=3), siRNA for *HDAC1* (n=4) and *HDAC3* (n=4). (**A-D**) Data (mean ± SEM) indicate WB immunoreactivity normalized to total protein loading (**A-D**) and to PPIA levels (**C-D**). *p < 0.05, **p < 0.01, ***p < 0.001, ****p < 0.0001 by one-way ANOVA, Dunnett's multiple comparisons (**A-B**), Uncorrected Fisher's LSD (**C**) or Tukey's multiple comparisons (**D**) post-hoc tests.

Figure 2. SAHA increases PPIAK125ac and reduces cytoplasmic TDP-43 in PBMCs of ALS patients. Electropherogram (**A**) and virtual lane view (**B**) of the TDP-43 signal by capillary electrophoresis immunoassay (CEI) in cytoplasmic fractions of PBMCs from an ALS patient (red line) and a healthy control (black line). Peaks for TDP-43, TDP-35CTF and TDP-25CTF are indicated. (**C-E**) CEI analysis of cytoplasmic (Cyt.) TDP-43 and TDP-35CTF (**C-D**), and nuclear (Nuc.) PPIAK125ac (**E**) in PBMCs of ALS patients (n=9) and healthy controls (n=54). Data (mean ± SEM) indicate CEI immunoreactivity normalized to total protein (**C-E**) and to PPIA levels (**E**). **p < 0.01, ****p < 0.0001 by Mann Whitney test. (**F-J**) CEI analysis of nuclear PPIAK125ac (**F**), nuclear (Nuc.) and cytoplasmic (Cyt.) PPIA **(G-H)**, and cytoplasmic (Cyt.) TDP-43 and TDP-35CTF (**I-J**) in the cultured PBMCs of the same ALS patients treated or not with 1 μM SAHA. (**F**) Data (mean ± SEM; n=3 technical replicates derived from pools of the 9 ALS patients Untr or SAHA treated) indicate CEI immunoreactivity normalized to total protein and to PPIA levels. ***p < 0.001 by Student's *t* test. (**G-J**) Data (mean ± SEM; n=9) are shown as slope chart and indicate CEI immunoreactivity of SAHA-treated PBMCs, normalized to total protein loading, in comparison with the relative untreated sample. The black slope chart indicates the mean value for each protein target. *p < 0.05, **p < 0.01 by Student's paired *t* test.

Figure 3. Homozygous Thy1-hTDP-43 mouse is a severe model of TDP-43 proteinopathy. (**A-Q**) Thy-hTDP-43 mice were characterized at pre-symptomatic (PS), disease onset (Ons) and symptomatic (Sym) stages for ALS pathological markers. (**A,C**) Quantification of Nissl-stained motor neurons (MNs > 250 μm^2) and CD11b-stained microglia in lumbar spinal cord hemisections from non-transgenic (Ntg) and Thy1-hTDP-43 mice at Ons and Sym stage. Data are mean ± SEM (n=3). **p < 0.01 and ***p < 0.001 versus Ntg, °°p < 0.01 versus Ons by one-way ANOVA, Tukey's multiple comparisons. Representative Nissl- and CD11b-stained lumbar spinal cord sections are shown. Scale bar 50 μm. (**B**) NfL plasma levels in Ntg (n=5) and Thy1-hTDP-43 mice at Ons and Sym stages (n=11). Data are mean ± SEM. *p < 0.05 and ****p < 0.0001 versus Ntg, °°°°p < 0.0001 versus Ons by one-way ANOVA, Tukey's multiple comparisons. (**D-F**) Analysis of nuclear (Nuc.)

and cytoplasmic (Cyt.) TDP-43 (**D**), cytoplasmic (Cyt) TDP-35CTF (**E**) and insoluble (Ins.) pTDP-43 (**F**) in spinal cord of Thy1-hTDP-43 mice at PS, Ons and Sym stages. Data (mean ± SEM; n=4-5 in each group) indicates immunoreactivity by dot blot (**D,F**) or WB (**E**) normalized to total protein loading. *p < 0.05, **p < 0.01 and ****p < 0.0001 versus PS, °°°p < 0.001 versus Ons by one-way ANOVA, Tukey's multiple comparisons (**D**) or Uncorrected Fisher's LSD (**E,F**) post hoc test. (**G**) Diagram illustrating skiptic exon (right) and representative lanes of Ube3C skiptic exon from acrylamide gel in spinal cord of Thy1-hTDP-43 mice at PS and Sym stages (left). **(H-K)** Semi quantitative PCR of Ankrd42 (**H**), Pacrgl (**I**), Slc6a6 (**J**) and Herc2 (**K**) skiptic exons in spinal cord of Thy1-hTDP-43 mice at PS, Ons and Sym stages. Data (mean ± SEM; n =5 in each group) are expressed as PEE. **p < 0.01, ***p < 0.001 and ****p < 0.0001 versus PS, °p < 0.05 and °°p < 0.01 versus Ons by one-way ANOVA, Tukey's multiple comparisons. (**L-M**) Analysis of nuclear (Nuc.) and cytoplasmic (Cyt.) PPIA (**L**) and nuclear (Nuc.) PPIAK125ac (**M**) in spinal cord of Thy1-hTDP-43 mice at PS, Ons and Sym stages. Data (mean ± SEM; n=3-5 per group) indicate immunoreactivity by dot blot (**L**) or CEI (**M**) normalized to total protein loading (**L-M**) and to PPIA (**M**) levels. *p < 0.05, **p < 0.01 versus PS by one-way ANOVA, Uncorrected Fisher's LSD post-hoc test. (**N-P**) Analysis of PPIA (**N**), pTDP-43 (**O**) and acetyl tubulin (Tubulin ac) **(P)** in sciatic nerve (Sci.) of Ntg (n=4-6) and Thy1-hTDP-43 mice at Ons (n=4-5). Data (mean ± SEM) indicate dot blot immunoreactivity normalized to total protein loading (**N-P**) and to tubulin (**P**) levels. *p < 0.05, ***p < 0.001 by Student's *t* test. (**Q**) RT-PCR for *AChR γ*-subunit in gastrocnemius muscle of Thy1-hTDP-43 mice at PS, Ons and Sym stages (n=3-5 in each group). Data (mean ± SEM) are normalized to *β-actin* and expressed as relative mRNA expression. *p < 0.05 versus PS, ° p < 0.05 versus Ons by one-way ANOVA with Tukey's multiple comparisons.

Figure 4. SAHA reduces neurodegeneration, TDP-43 pathology and peripheral nerve pathological markers in Thy1-hTDP-43 mouse at an early disease stage. (A) Scheme of SAHA treatment in homozygous Thy1-hTDP-43 mice. Mice were treated intraperitoneally with 50 mg/kg of SAHA from 7 days of age, every three days and sacrificed at 14 days for further analysis**. (B,D)** NfL **(B)** and MMP-9 **(D)** plasma levels in Thy1-hTDP-43 mice treated (n=5-10) or not (n=5-9) with SAHA. **(C)** RT-PCR for *Map-2* in spinal cord of Thy1-hTDP-43 mice treated (SAHA; n=4) or not (vehicle; n=5) with SAHA. Data are normalized to *β-actin* and expressed as relative mRNA expression. **(E-G)** Analysis of nuclear (Nuc.) and cytoplasmic (Cyt.) TDP-43 **(E),** cytoplasmic (Cyt.) TDP-35CTF **(F)** and insoluble (Ins.) pTDP-43 **(G)** in spinal cord of Thy1-hTDP-43 mice treated (n=5-6) or not (n=4-6) with SAHA. Data indicates dot blot **(E,G)** and WB **(F)** immunoreactivity normalized to total protein loading. **(H-J)** Semi quantitative PCR for Plod1 **(H)**, Pex16 **(I)**, and Herc2 **(J)** skiptic exons in spinal cord of Thy1-hTDP-43 mice treated (n=4) or not (n=6) with SAHA. Data are expressed as PEE. **(K-L)** Analysis of nuclear (Nuc.) PPIAK125ac **(K)**, nuclear (Nuc.) and cytoplasmic (Cyt.) PPIA **(L)** in spinal cord of Thy1-hTDP-43 mice treated (n=5-6) or not (n=4-5) with SAHA. Data indicates CEI **(K)** or dot blot **(L)** immunoreactivity normalized to total protein loading **(K-L)** and to PPIA levels **(K)**. **(M-O)** Analysis of PPIA **(M)**, pTDP-43 **(N)** and acetyl tubulin (Tubulin ac) **(O)** in sciatic nerve (Sci.) of Thy1-hTDP-43 mice treated (n=3-6) or not (n=5-6) with SAHA. Data indicates dot blot immunoreactivity normalized to

total protein loading **(M-O)** and to tubulin **(O)** levels. **(P)** RT-PCR for *AChR* γ-subunit in gastrocnemius muscle of Thy1-hTDP-43 mice treated (n=6) or not (n=5) with SAHA. Data are normalized to *β-actin* and expressed as relative mRNA expression. **(B-P)** Data are mean ± SEM. *p < 0.5, **p < 0.01, ***p < 0.001 by Student's *t* test.

Figure 5. Over time, SAHA maintains low NfL levels, but the effect on most of the other biomarkers is mitigated. (A) Scheme of SAHA treatment in homozygous Thy1-hTDP-43 mice. Mice were treated intraperitoneally with 50 mg/kg of SAHA from 7 days of age, every three days and sacrificed at 17 days for further analysis. **(B)** Body weight curve of Thy1-hTDP-43 mice treated (n=12) or not (n=13) with SAHA. Data (mean ± SEM) are expressed as percentage of body weight from 7 to 16 days of age relative to the starting body weight at 7 days of age; ***p < 0.001 vehicle versus SAHA by two-way ANOVA for repeated measures followed by Sidak's post hoc test. **(C,E)** NfL **(C)** and MMP-9 **(E)** plasma levels in Thy1-hTDP-43 mice treated (n=12) or not (n=9) with SAHA. **(D)** RT-PCR for *Map-2* in spinal cord of Thy1-hTDP-43 mice treated (n=6) or not (n=5) with SAHA. Data are normalized to *β-actin* and expressed as relative mRNA expression. **(F-H)** Analysis of nuclear (Nuc.) and cytoplasmic (Cyt.) TDP-43 **(F)**, cytoplasmic (Cyt.) TDP-35CTF **(G)** and insoluble (Ins.) pTDP-43 **(H)** in spinal cord of Thy1-hTDP-43 mice treated (n=3-6) or not (n=4-6) with SAHA. Data indicates dot blot **(F,H)** and WB **(G)** immunoreactivity normalized to total protein loading. **(I-K)** Semi quantitative PCR for Plod1 **(I)**, Pex16 **(J)** and Herc2 **(K)** skiptic exons in spinal cord of Thy1-hTDP-43 mice treated (n=6) or not (n=6) with SAHA. Data are expressed as PEE. **(L-M)** Analysis of nuclear (Nuc.) PPIAK125ac **(L)**, nuclear (Nuc.) and cytoplasmic (Cyt.) PPIA (**M)** in spinal cord of Thy1-hTDP-43 mice treated (n=5-6) or not (n=4-5) with SAHA. Data indicates CEI **(L)** and dot blot **(M)** immunoreactivity normalized to total protein loading **(L-M)** and to PPIA levels **(L)**. **(N-P)** Analysis of PPIA **(N)**, pTDP-43 **(O)** and acetyl tubulin (Tubulin ac) **(P)** in sciatic nerve (Sci.) of Thy1-hTDP-43 mice treated (n=5-6) or not (n=4-6) with SAHA. Data indicates dot blot immunoreactivity normalized to total protein loading **(N-P)** and to tubulin levels **(P)**. **(Q)** RT-PCR for *AChR γ*-subunit in gastrocnemius muscle of Thy1-hTDP-43 mice treated (n=4) or not (n=3) with SAHA. Data are normalized to *β-actin* and expressed as relative mRNA expression. **(C-Q)** Data are mean ± SEM. *p < 0.05, **p < 0.01, ****p < 0.0001 by Student's *t* test.

Figure 6. SAHA+Arimoclomol enhances the positive effect on markers of neuromuscular pathology. (A) Scheme of SAHA+Arimoclomol (SAHA+Arim.) treatment combination in homozygous Thy1-hTDP-43 mice. Mice were treated intraperitoneally with 50 mg/kg of SAHA and 10 mg/kg of arimoclomol, from 7 days of age, every three days and sacrificed at 17 days for further analysis. **(B)** Level of HSP70 in spinal cord of Thy1-hTDP-43 mice treated (n=6) or not (n=4) with SAHA+Arim. Data indicates WB immunoreactivity normalized to total protein loading. **(C,E)** NfL **(C)** and MMP-9 **(E)** plasma levels in Thy1-hTDP-43 mice treated (n=5-12) or not (n=10-12) with SAHA+Arim. **(D)** RT-PCR for *Map-2* in spinal cord of Thy1-hTDP-43 mice treated (n=5) or not (n=4) with SAHA+Arim. Data are normalized to *β-actin* and expressed as relative mRNA expression. **(F-H)** Analysis of nuclear (Nuc.) and cytoplasmic (Cyt.) TDP-43 **(F)**, cytoplasmic (Cyt.) TDP-

35CTF **(G)** and insoluble (Ins.) pTDP-43 **(H)** in spinal cord of Thy1-hTDP-43 mice treated (n=5-6) or not (n=4-5) with SAHA+Arim. Data indicates dot blot **(F,H)** and WB **(G)** immunoreactivity normalized to total protein loading. **(I-J)** Semi quantitative PCR for Ube3C **(I)** and Slc6a6 **(J)** skiptic exons in spinal cord of Thy1-hTDP-43 mice treated (n=5) or not (n=5) with SAHA+Arim. Data are expressed as PEE. **(K-L)** Analysis of nuclear (Nuc.) PPIAK125ac **(K)**, nuclear (Nuc.) and cytoplasmic (Cyt.) PPIA (**L)** in spinal cord of Thy1-hTDP-43 mice treated (n=5-6) or not (n=4-5) with SAHA+Arim. Data indicates CEI **(K)** and dot blot **(L)** immunoreactivity normalized to total protein **(K-L)** and to PPIA levels **(K)**. **(M-O)** Analysis of PPIA **(M)**, acetyl tubulin (Tubulin ac) **(N)** and pTDP-43 **(O)** in sciatic nerve (Sci.) of Thy1-hTDP-43 mice treated (n=5-6) or not (n=5-6) with SAHA+Arim. Data indicates dot blot immunoreactivity normalized to total protein loading **(M-O)** and to tubulin levels **(N)**. **(P)** RT-PCR for *AChR γ*-subunit in gastrocnemius muscle of Thy1-hTDP-43 mice treated (n=6) or not (n=3) with SAHA+Arim. Data are normalized to *β-actin* and expressed as relative mRNA expression. **(B-P)** Data are mean ± SEM. *p < 0.5, **p < 0.01, ****p < 0.0001 by Student's *t* test.

Supplementary Figure 1. The effect of SAHA is dose-dependent in an *in vitro* model of TDP-43 proteinopathy. (A-B) Quantification of nuclear (Nuc). levels of TDP-43 **(A)** and TDP-35CTF **(B)** in control (Ctrl; n=5-6) and serum-deprived HEK293 cells, subjected or not (Starv. Untr; n=6) to overnight treatment with 0.6 μM and 1 μM concentrations of SAHA (Starv. SAHA; n=5-6). **(C-D)** Quantification of cytoplasmic (Cyt.) levels of TDP-43 **(C)** and TDP-35CTF **(D)** in control (Ctrl; n > 6) and serum-deprived HEK293 cells, subjected or not (Starv. Untr; n > 6) to overnight treatment with 0.6 μM and 1 μM concentrations of SAHA (Starv. SAHA; n=6). Data (mean ± SEM) indicates CEI **(A-B)** and WB **(C-D)** immunoreactivity normalized to total protein loading. *p < 0.05, **p < 0.01, ***p < 0.001, ****p < 0.0001 by one-way ANOVA with Uncorrected Fisher's LSD **(A-B)** and Dunnett's multiple comparisons (**C-D**) post hoc tests.

Supplementary Figure 2. Characterisation of acetyl-PPIA antibody. (A) Representative dot blot of different concentrations of the recombinant peptide WLDGKHVVFG, acetylated or not-acetylated at the K residue, after anti-PPIAK125ac antibody hybridization. **(B)** Representative WB after hybridization with anti-PPIAK125ac and PPIA antibody of spinal cord tissues from PPIA knock-out (PPIA-/-) mice and relative Ntg controls, lysate of serum-deprived HEK293 cells (Starvation) and control (Ctrl) and human PBMCs from ALS patients. **(C)** Representative electropherogram following PPIAK125ac and PPIA hybridization in the same capillary through CEI in spinal cord of Ntg mice. The peak of PPIA (grey) includes that of PPIAK125ac (orange).

Supplementary Figure 3. Analysis of a set of skiptic exons in the spinal cord of homozygous Thy1-hTDP-43 mice. (A-C) Semi quantitative PCR of Ube3C **(A)**, Plod1 **(B)**, Pex16 **(C)** skiptic exons in spinal cord of Thy1-hTDP-43 at pre-symptomatic (PS, 7 days of age), onset (Ons, 14 days of age) and symptomatic (Sym, 17 days of age) stage. Data (mean ± SEM; n =5 in each experimental group) are expressed as PEE. *p < 0.05,

p < 0.01, ***p < 0.001, ****p < 0.0001 versus PS, ° p < 0.05, °°° p < 0.001 versus Ons by one-way ANOVA with Tukey's multiple comparisons. **(D-G) Semi quantitative PCR for Ankrd42 **(D)**, Ube3C **(E)**, Slc6a6 **(F)** and Pacrgl **(G)** skiptic exon in spinal cord of Thy1-hTDP-43 mice treated (SAHA; n=4) or not (Vehicle; n=6) with SAHA at disease onset. Data (mean ± SEM) are expressed as PEE. **(H-K)** Semi quantitative PCR for Ankrd42 **(H)**, Ube3C **(I)**, Slc6a6 **(J)** and Pacrgl **(K)** skiptic exon in spinal cord of Thy1-hTDP-43 mice treated (SAHA; n=6) or not (Vehicle; n=6) with SAHA at symptomatic stage. Data (mean ± SEM) are expressed as PEE. **(L-P)** Semi quantitative PCR for Plod1 **(L)**, Pex16 **(M)**, Ankrd42 **(N)**, Pacrgl **(O)** and Herk2 **(P)** skiptic exon in spinal cord of Thy1-hTDP-43 mice treated (SAHA+Arim.; n=5) or not (Vehicle; n=5) with SAHA+Arim. at symptomatic stage. Data (mean ± SEM) are expressed as PEE.

Supplementary Figure 4. Dose response effect of SAHA treatment in homozygous Thy1-hTDP-43 mice. (**A-B**) Scheme of SAHA treatment in homozygous Thy1-hTDP-43 mice. Mice were treated intraperitoneally with 50 mg/kg of SAHA, from 7 days of age, daily (SAHA #1)(**A**) or every three days (SAHA #2)(**B**) and sacrificed at 14 days for further analysis. (**C**) NfL plasma levels in homozygous Thy1-hTDP-43 mice treated with SAHA daily (SAHA #1; n=5), every three days (SAHA #2; n=5) or vehicle (Veh; n=9). Data are mean ± SEM. **p < 0.01, ****p < 0.0001 versus Veh by one-way ANOVA with Tukey's multiple comparisons. (**D**) Levels of cytoplasmic (Cyt.) C-terminal fragment at 35 kDa (TDP-35CTF) in spinal cord of homozygous Thy1-hTDP-43 mice treated with SAHA daily (SAHA #1; n=4), every three days (SAHA #2; n=6) or vehicle (Veh; n=4). Data (mean ± SEM) indicates WB immunoreactivity normalized to total protein loading. *p < 0.05 versus Veh by one-way ANOVA with Tukey's multiple comparisons.

Supplementary Figure 5. Effect of SAHA and SAHA+Arimoclomol combination on the expression of Hdacs in lumbar spinal cord of Thy1-hTDP-43 mice. (**A-O**) RT-PCR for *Hdac1*, *Hdac2*, *Hdac3*, *Hdac4* and *Hdac6* in spinal cord of Thy1-hTDP-43 mice treated with SAHA or vehicle and analysed at disease onset (n=4-5 in each experimental group) (**A-E**), at symptomatic stage (n=5-6 in each experimental group) (**F-J**) or treated with SAHA+Arim. combination and analysed at symptomatic stage (n=5 in each experimental group) (**K-O**). Data (mean ± SEM) are normalized to *β-actin* and expressed as relative mRNA expression. *p < 0.05, **p < 0.01 by Student's *t* test.

Supplmentary Figure 6. Arimoclomol has no effect on insoluble TDP-43 and markers of neuromuscular pathology. (A) Scheme of arimoclomol (Arim.) and SAHA+arimoclomol (SAHA+Arim.) combination treatment in homozygous Thy1-hTDP-43 mice. Mice were treated intraperitoneally with 10 mg/kg of Arimoclomol or 50 mg/kg of SAHA and 10 mg/kg of arimoclomol, from 7 days of age, every three days and sacrificed at 17 days for further analysis. **(B-C)** Analysis of acetyl tubulin (Tubulin ac) **(B)** and pTDP-43 **(C)** in sciatic nerve (Sci.) of Thy1-hTDP-43 mice treated with Arim. (n=4-5) or SAHA+Arim (n=6-5) or not (n=6-5). Data indicates dot blot immunoreactivity normalized to total protein loading **(B-C)** and to tubulin levels **(B)**. *p < 0.05 versus Veh and °°p < 0.01 versus Arim. by one-way ANOVA with Tukey's multiple comparisons. **(D)** Analysis of insoluble (Ins.) pTDP-43 in spinal cord of Thy1-hTDP-43 mice treated with

Arim. (n=5) or SAHA+Arim. (n=4) or not (n=6). Data indicates dot blot immunoreactivity normalized to total protein loading. **(E)** NfL plasma levels in Thy1-hTDP-43 mice treated with Arim. (n=6) or SAHA+Arim (n=5) or not (n=15). *$p < 0.05$ versus vehicle by one-way ANOVA with Tukey's multiple comparisons. **(F)** RT-PCR for *AChR γ*-subunit in gastrocnemius muscle of Thy1-hTDP-43 mice treated with Arim. (n=6) or SAHA+Arim. (n=6) or not (n=3). Data are normalized to *β-actin* and expressed as relative mRNA expression. *$p < 0.05$ versus vehicle by Student's *t* test.

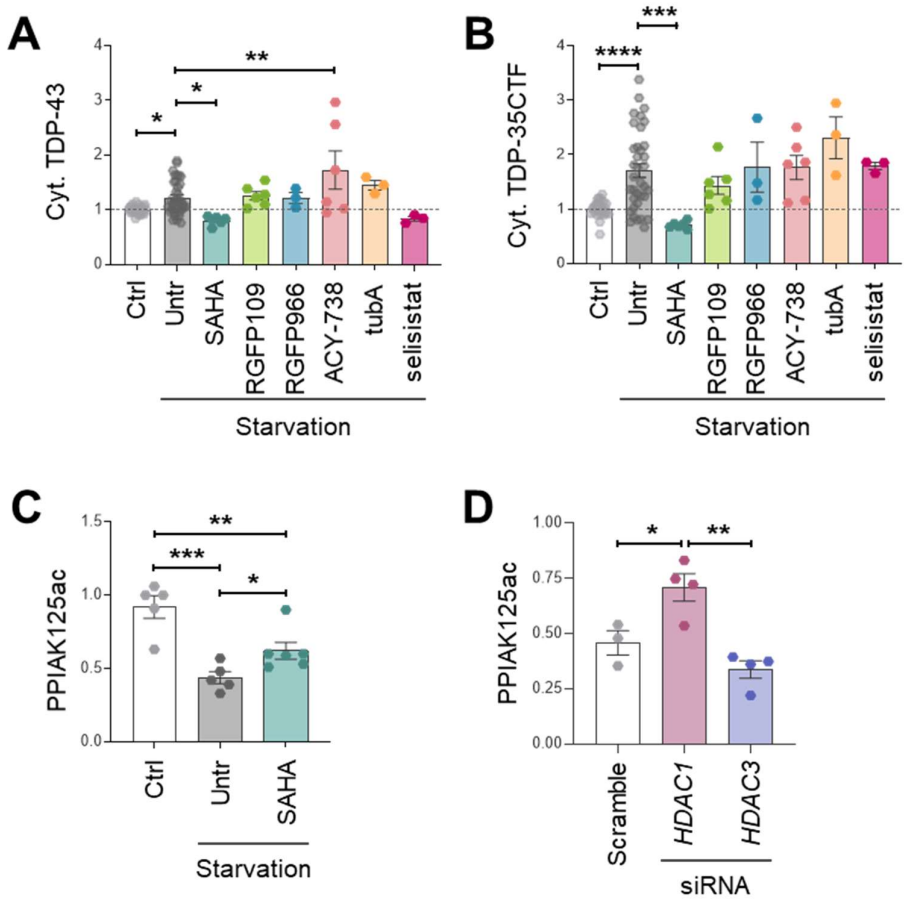
A
Cyt. TDP-43
Ctrl
Untr
SAHA
RGFP109
RGFP966
ACY-738
tubA
selisistat
Starvation
B
Cyt. TDP-35CTF
C
PPIAK125ac
D
Scramble
HDAC1
HDAC3
siRNA

Figure 1

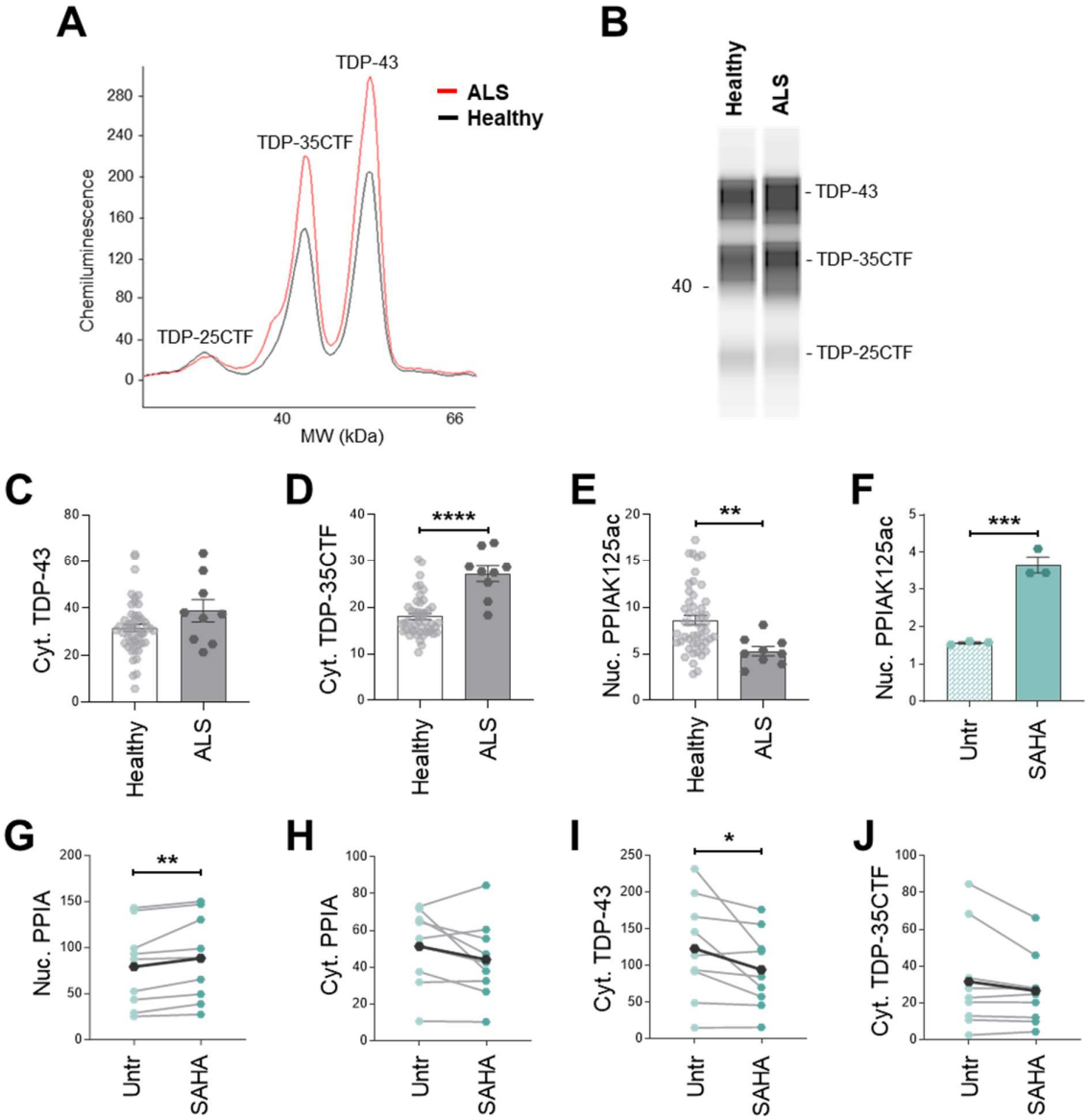
A
TDP-43
ALS
Healthy
TDP-35CTF
TDP-25CTF
Chemiluminescence
MW (kDa)
B
Healthy
ALS
- TDP-43
- TDP-35CTF
40 -
- TDP-25CTF
C
Cyt. TDP-43
Healthy
ALS
D
Cyt. TDP-35CTF
****
Healthy
ALS
E
Nuc. PPIAK125ac
**
Healthy
ALS
F
Nuc. PPIAK125ac
***
Untr
SAHA
G
Nuc. PPIA
**
Untr
SAHA
H
Cyt. PPIA
Untr
SAHA
I
Cyt. TDP-43
*
Untr
SAHA
J
Cyt. TDP-35CTF
Untr
SAHA

Figure 2

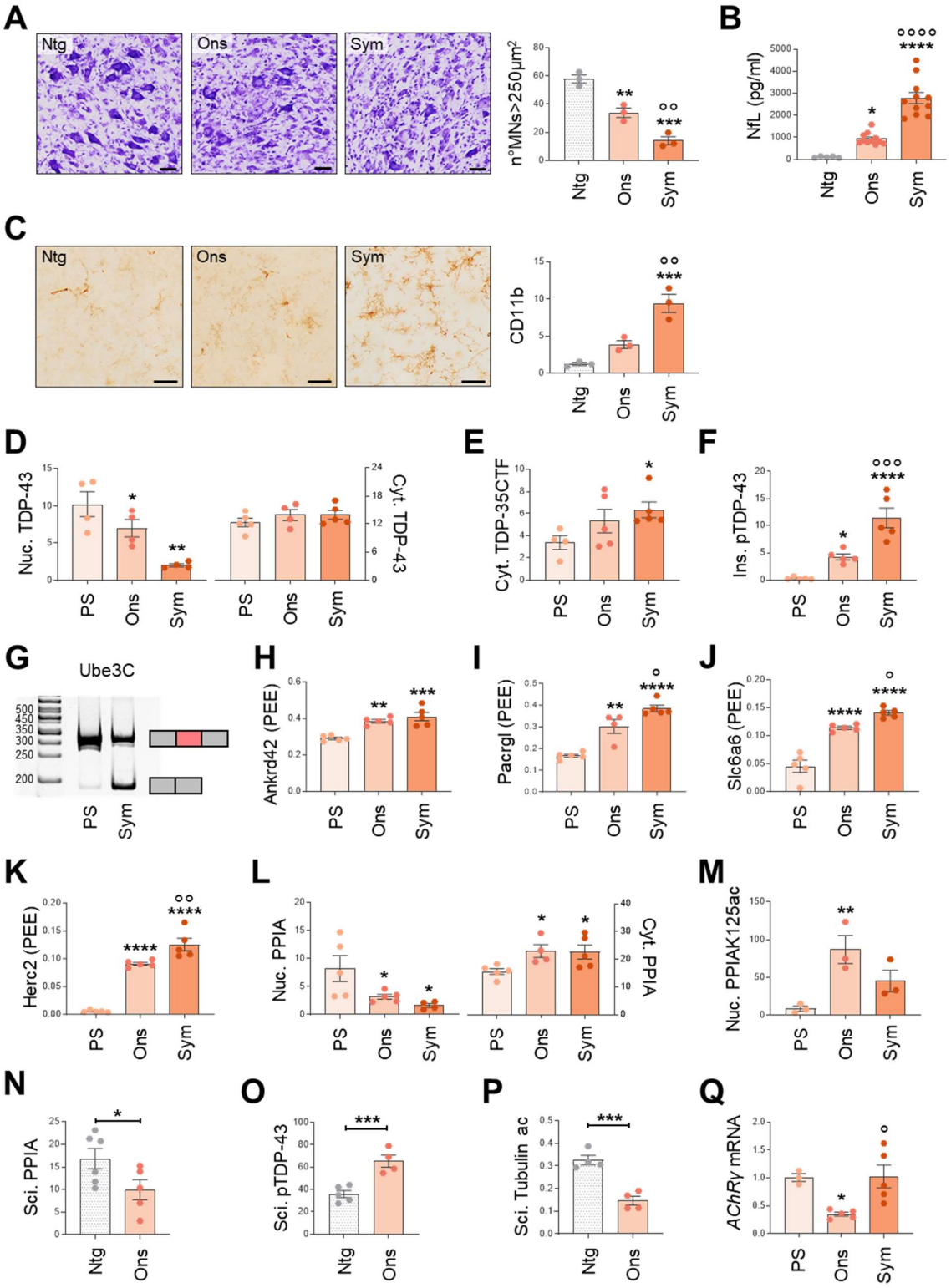
A
Ntg
Ons
Sym
n°MNs>250µm²
B
NfL (pg/ml)
C
CD11b
D
Nuc. TDP-43
Cyt. TDP-43
E
Cyt. TDP-35CTF
F
Ins. pTDP-43
G
Ube3C
H
Ankrd42 (PEE)
I
Pacrgl (PEE)
J
Slc6a6 (PEE)
K
Herc2 (PEE)
L
Nuc. PPIA
Cyt. PPIA
M
Nuc. PPIAK125ac
N
Sci. PPIA
O
Sci. pTDP-43
P
Sci. Tubulin ac
Q
AChRγ mRNA
PS
Ons
Sym

Figure 3

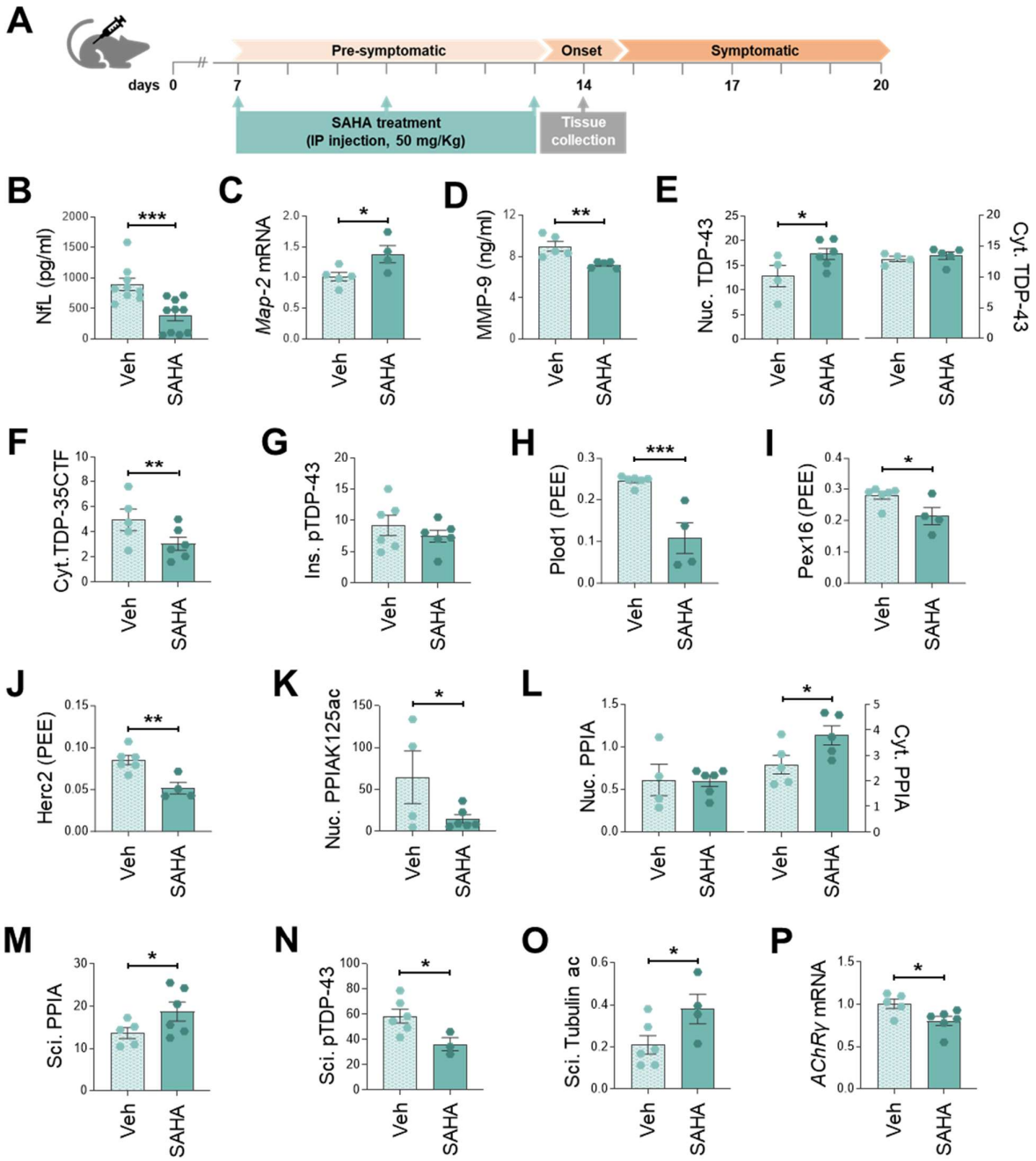
A
Pre-symptomatic
Onset
Symptomatic
days 0
7
14
17
20
SAHA treatment
(IP injection, 50 mg/Kg)
Tissue
collection
B
NfL (pg/ml)
C
Map-2 mRNA
D
MMP-9 (ng/ml)
E
Nuc. TDP-43
Cyt. TDP-43
F
Cyt.TDP-35CTF
G
Ins. pTDP-43
H
Plod1 (PEE)
I
Pex16 (PEE)
J
Herc2 (PEE)
K
Nuc. PPIAK125ac
L
Nuc. PPIA
Cyt. PPIA
M
Sci. PPIA
N
Sci. pTDP-43
O
Sci. Tubulin ac
P
AChRγ mRNA
Veh
SAHA

Figure 4

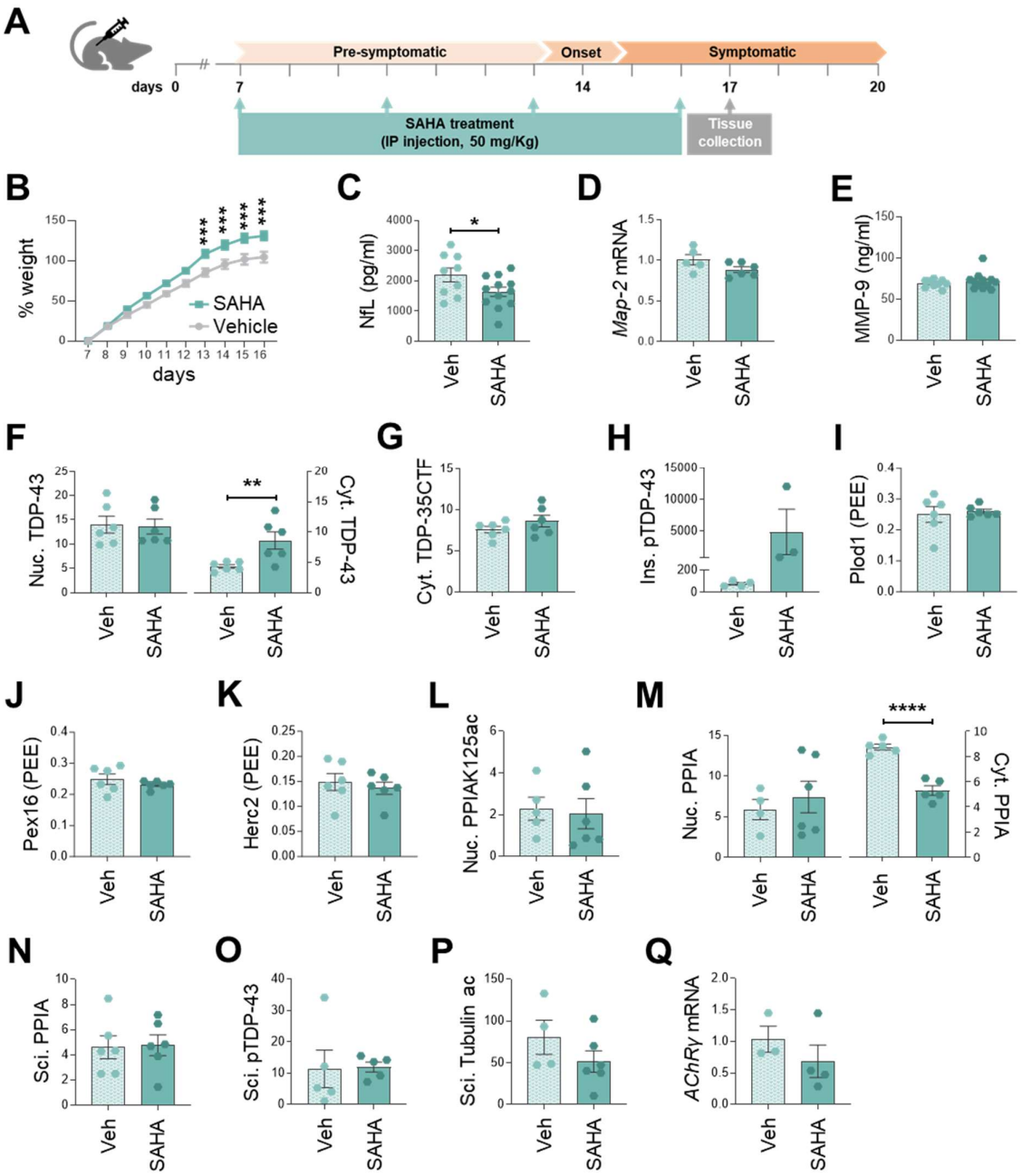
A
Pre-symptomatic
Onset
Symptomatic
days 0
7
14
17
20
SAHA treatment
(IP injection, 50 mg/Kg)
Tissue
collection
B
% weight
SAHA
Vehicle
days
C
NfL (pg/ml)
D
Map-2 mRNA
E
MMP-9 (ng/ml)
F
Nuc. TDP-43
Cyt. TDP-43
G
Cyt. TDP-35CTF
H
Ins. pTDP-43
I
Plod1 (PEE)
J
Pex16 (PEE)
K
Herc2 (PEE)
L
Nuc. PPIAK125ac
M
Nuc. PPIA
Cyt. PPIA
N
Sci. PPIA
O
Sci. pTDP-43
P
Sci. Tubulin ac
Q
AChRγ mRNA
Veh
SAHA

Figure 5

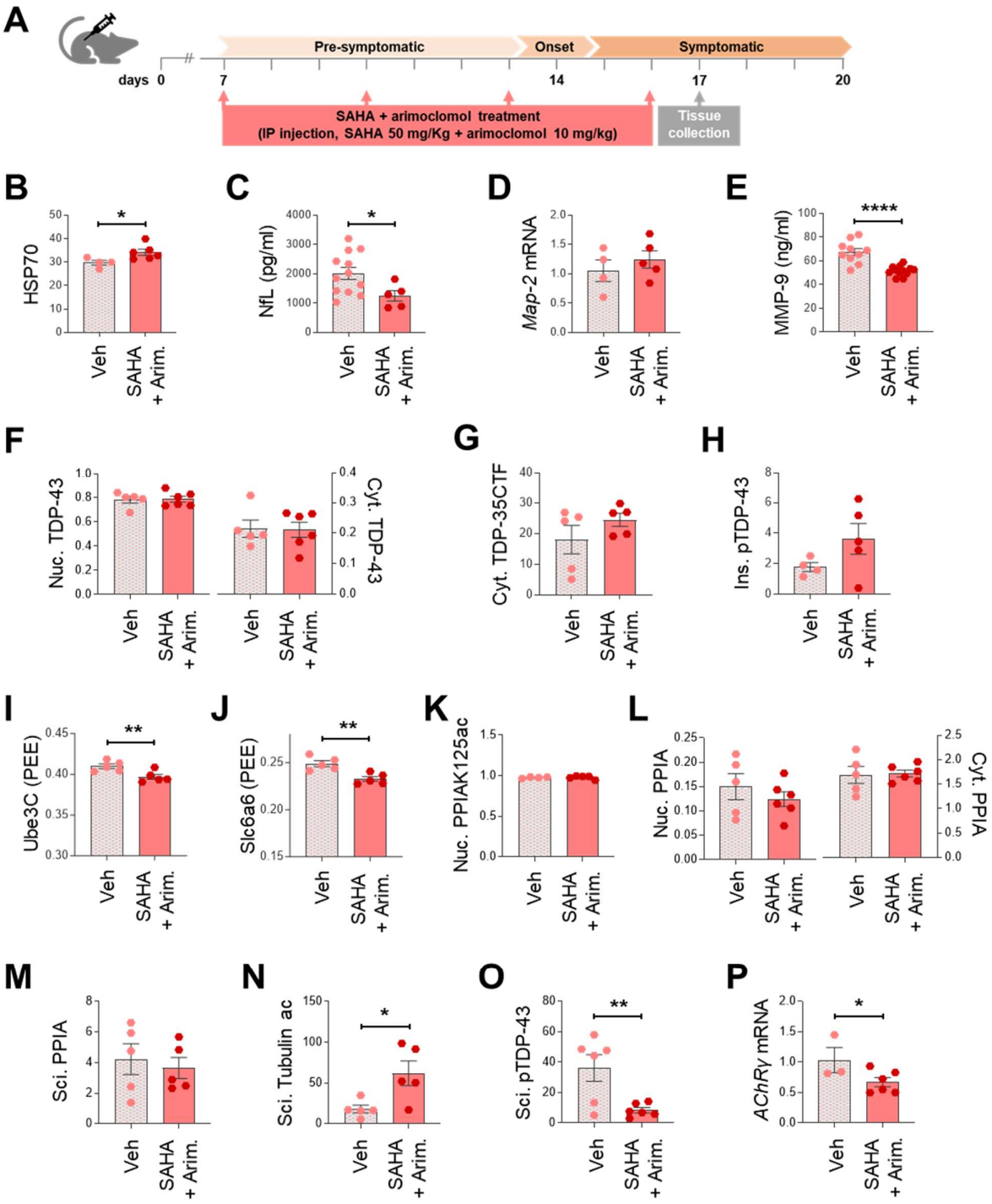
A
Pre-symptomatic
Onset
Symptomatic
days 0
7
14
17
20
SAHA + arimoclomol treatment
(IP injection, SAHA 50 mg/Kg + arimoclomol 10 mg/kg)
Tissue collection
B
HSP70
C
NfL (pg/ml)
D
Map-2 mRNA
E
MMP-9 (ng/ml)
F
Nuc. TDP-43
Cyt. TDP-43
G
Cyt. TDP-35CTF
H
Ins. pTDP-43
I
Ube3C (PEE)
J
Slc6a6 (PEE)
K
Nuc. PPIAK125ac
L
Nuc. PPIA
Cyt. PPIA
M
Sci. PPIA
N
Sci. Tubulin ac
O
Sci. pTDP-43
P
AChRγ mRNA
Veh
SAHA + Arim.

Figure 6

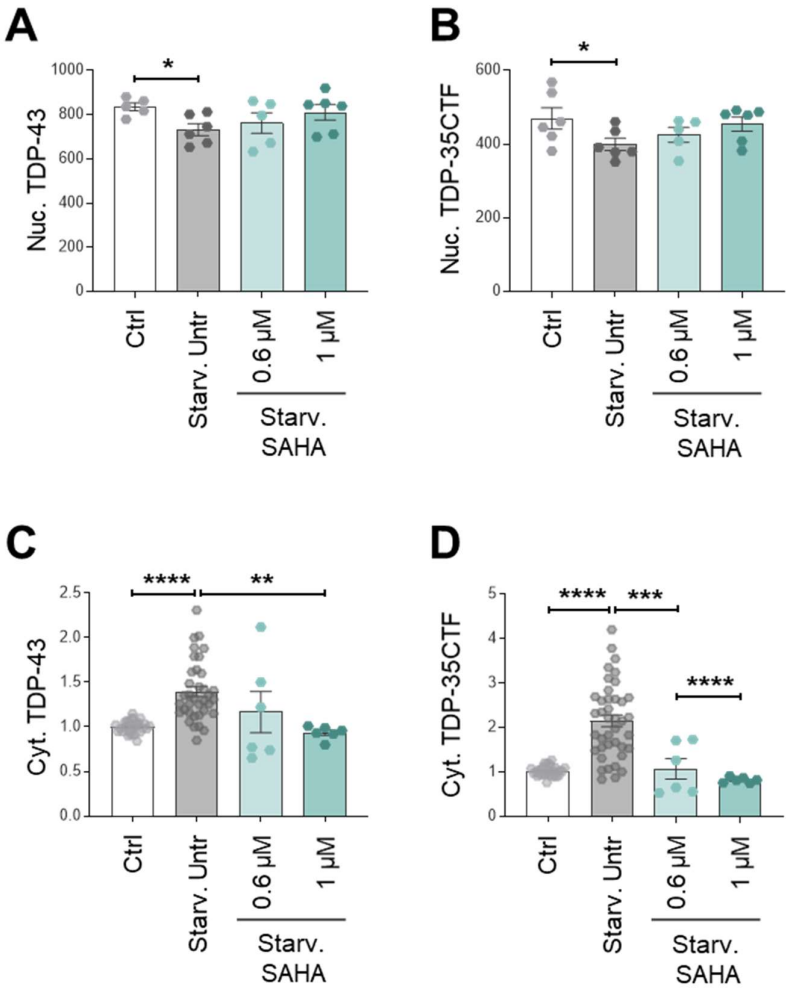

Supplementary Figure 1

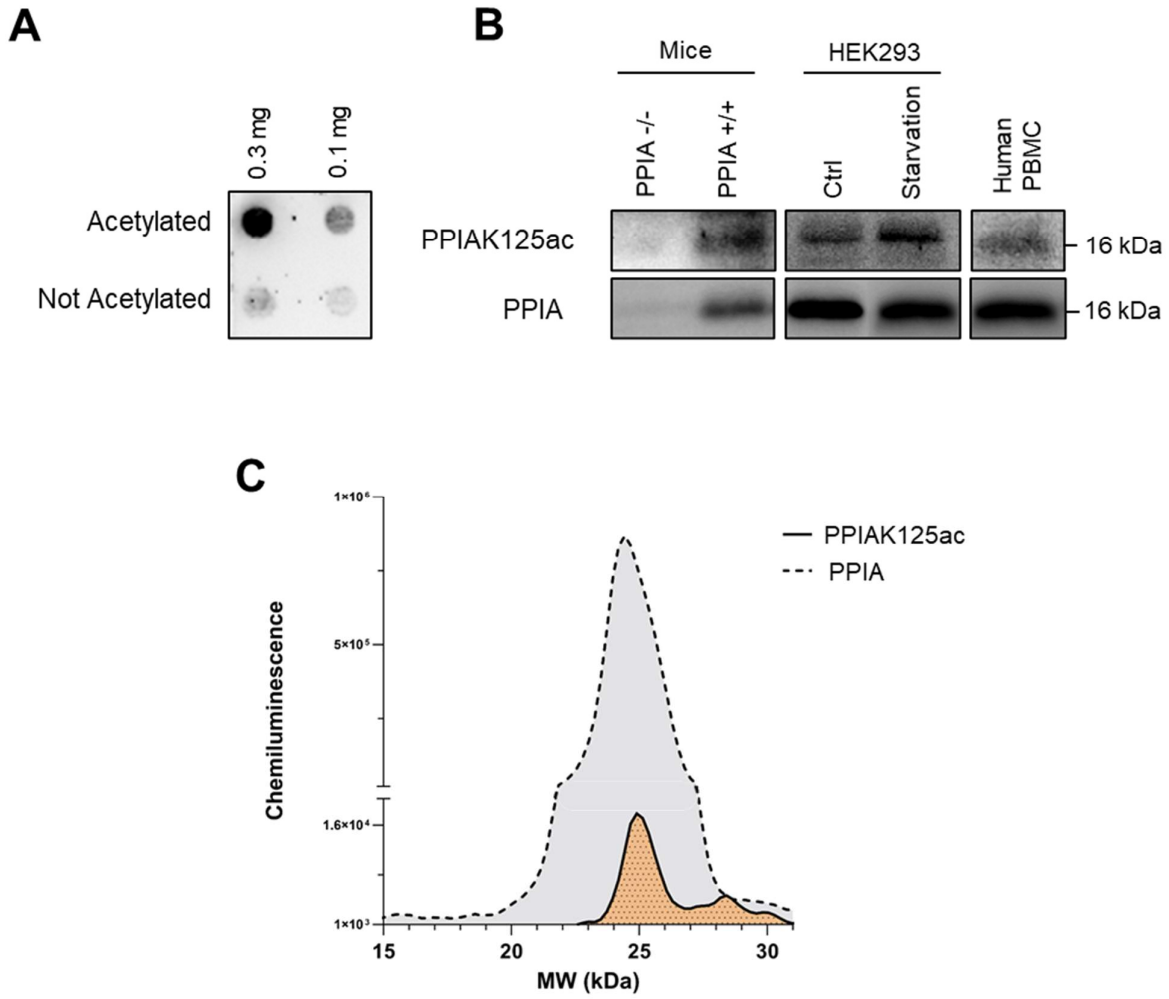

Supplementary Figure 2

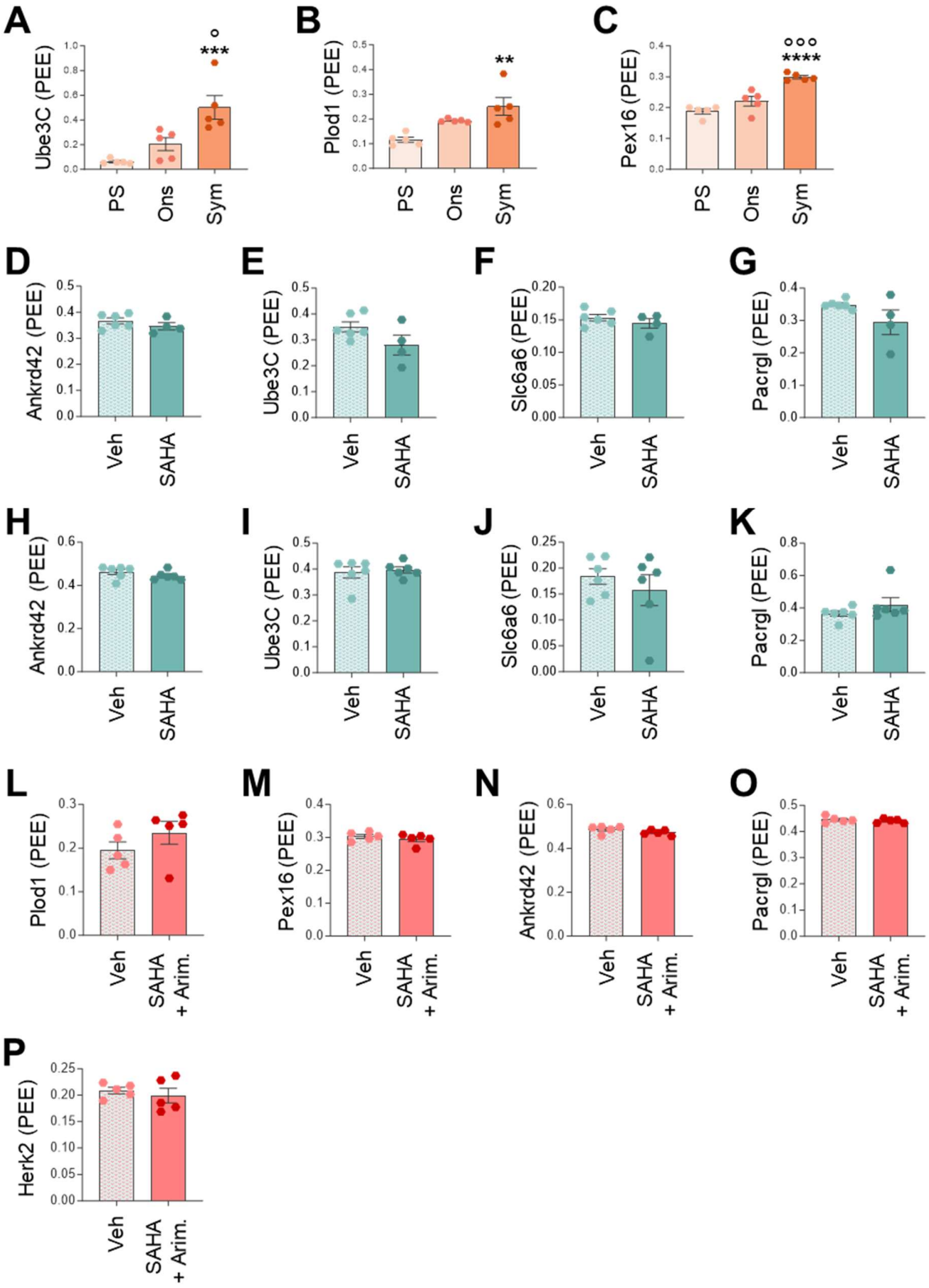

Supplementary Figure 3

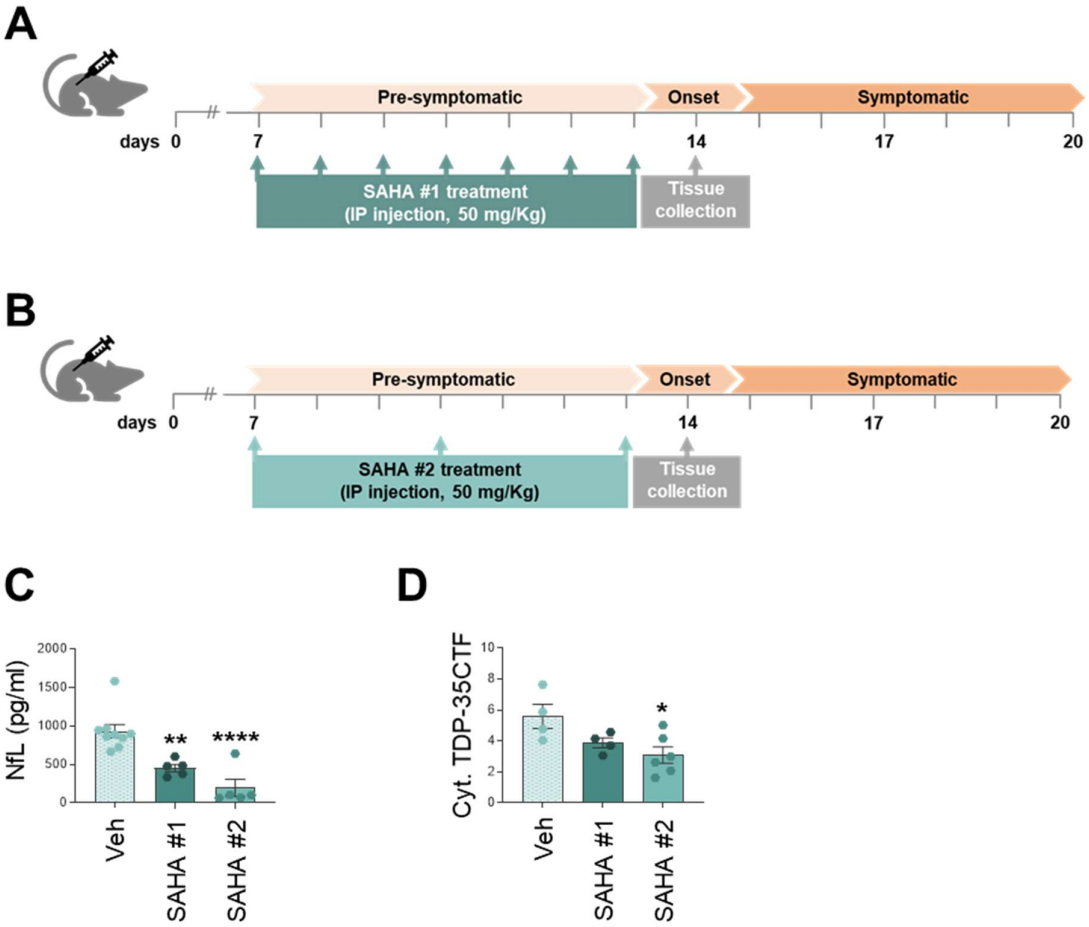

Supplementary Figure 4

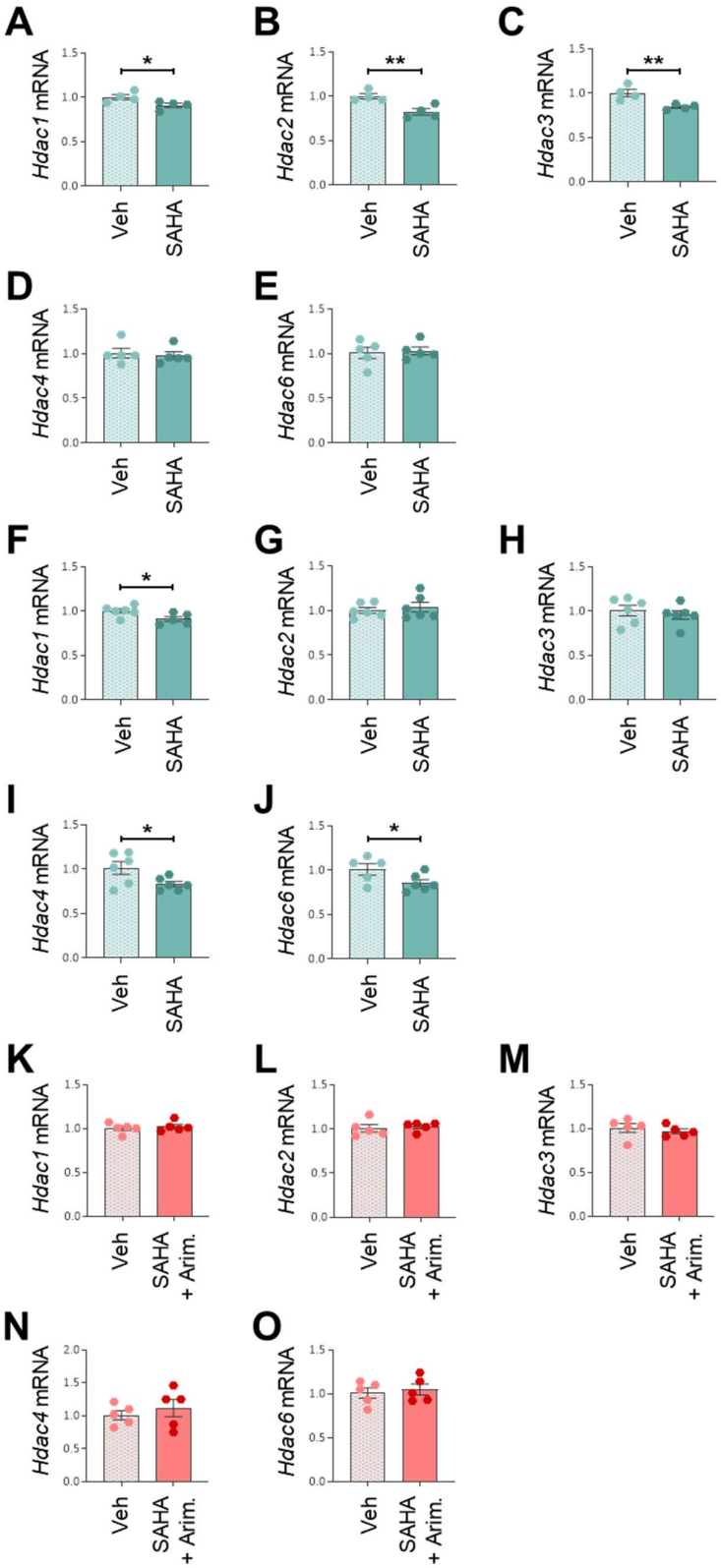

Supplementary Figure 5

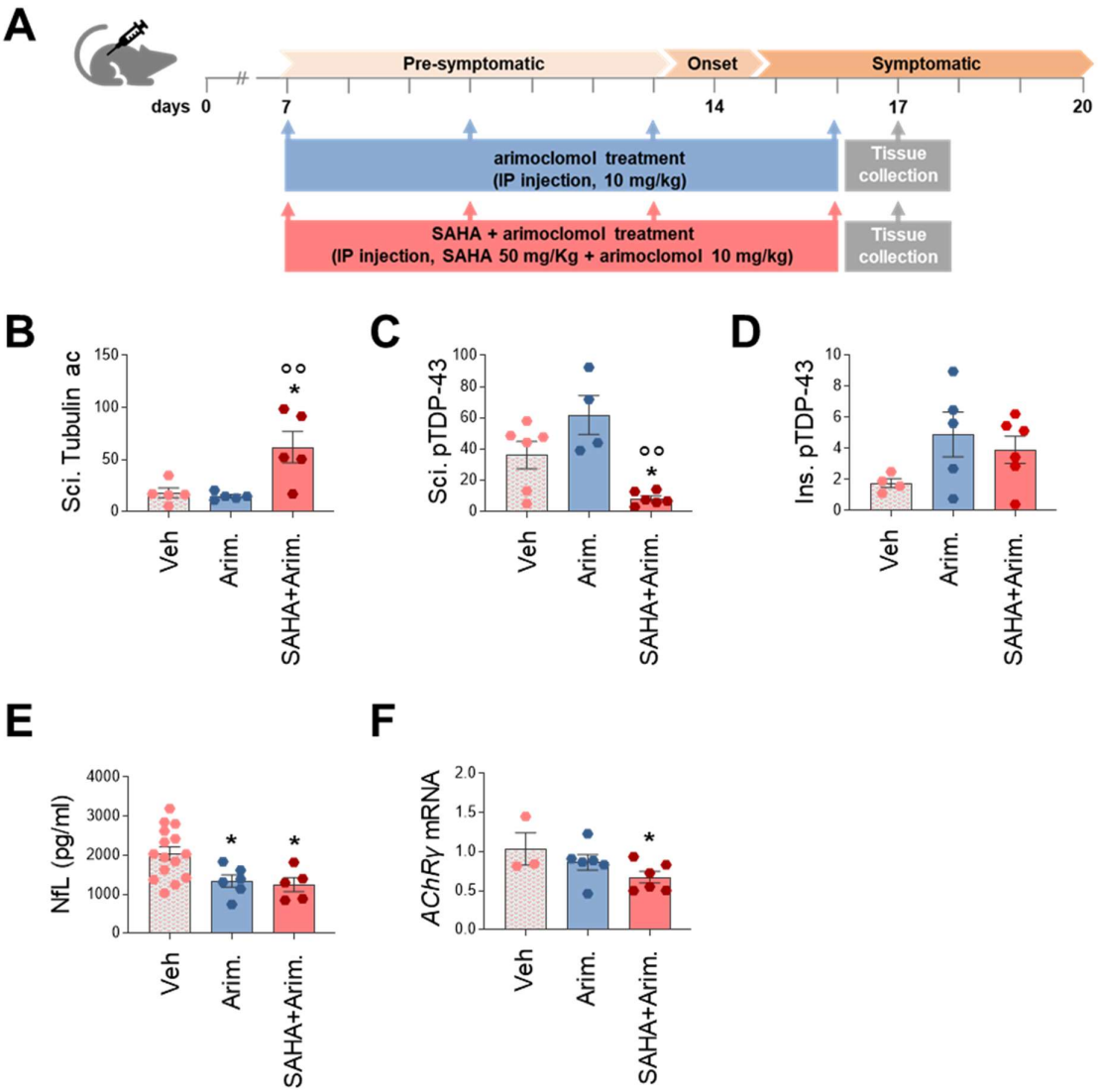

Supplementary Figure 6

Supplementary Table 1. Skiptic and cryptic primer sequences

Gene	Sequence 5'-3'
Ankrd42[a]	Forward: TCAATGGAGCCAACCTAGCA Reverse: GGCTTGTGTTGCACTGTTCAT
Herc2[a]	Forward: GGCTGCTAGACCACTCTGAT Reverse: TGACTTTGCCCACATCACCT
Pacrgl[a]	Forward: GGTCAAGGGTGCTCCTGAAA Reverse: AACCCCTACAGCACTCAACG
Pex16[a]	Forward: GTGCTGCTCAATGACGGGAT Reverse: ATGCCAGCCTTGAACCAGAT
Plod1[a]	Forward: CACCTGCTTTCCCTGGATAACT Reverse: ACTGGCCATAGTGTTCCATCTC
Slc6a6[a]	Forward: CATGACCTCACTGGGAAGCTAT Reverse: ATAGACCAAAAGGTGGGCAGC
Ube3c[a]	Forward: TGGATGGATCAGAGAGACTGACA Reverse: TGGTTTTAGGACATTCTCCAGC
2610507B11Rik[b]	Forward: CAGAACACAGAGGTGGAGCAA Reverse: AGAGGTAGCCACCTTAAGAACC
A230046K03Rik[b]	Forward: CCTTCCTACAGCAGAAAGCTCA Reverse: TGGTGAGGTCTTCAGCAAATGT
Adipor2[b]	Forward: GCTCAGAAAAGGGCACCAAC Reverse: CGTTCCATAGCATGATGGGC
Adnp2[b]	Forward: TCCAAAATGTTTCAAATTCCTGTGC Reverse: GGAGAAACATCTCCCCACGA
Celf5[b]	Forward: CGGAAGCTGTTCGTGGGTAT Reverse: GCCTCTGTGTGGGAAGAAAAC

[a] skiptic primer sequences
[b] cryptic primer sequences

Supplementary Table 1